Journal of the American Chemical Society 133: 986- 997 (2011)

Original design of an oxygen-tolerant [NiFe] hydrogenase: Major effect of a valine-to-cysteine mutation near the active site

Pierre-Pol Liebgott[a], Antonio L. de Lacey[b], Bénédicte Burlat[a,d], Laurent Cournac[c,d,e], Pierre Richaud[c,d,e], Myriam Brugna[a] , Victor M. Fernandez[b], Bruno Guigliarelli[a,d], Marc Rousset[a], Christophe Léger[a], Sébastien Dementin[a*]

[a] CNRS, Laboratoire de Bioénergétique et Ingénierie des Protéines, Institut de Microbiologie de la Méditerranée, 31 chemin Joseph Aiguier, 13402 Marseille Cedex 20, France.

[b] Instituto de Catalisis, CSIC, c/ Marie Curie 2, 28049 Madrid, Spain

[c]CEA, DSV, IBEB, Laboratoire de Bioénergétique et Biotechnologie des Bactéries et Microalgues, 13108 Saint-Paul-lez-Durance, France.

[d] Aix-Marseille Université, 3 place Victor-Hugo 13331 Marseille, France.

[e] CNRS, UMR Biologie Végétale et Microbiologie Environnementales, 13108 Saint Paul Lez Durance, France.

[*] corresponding author : Sébastien Dementin

Tel: +33 4 91164209

E-mail address: dementin@ifr88.cnrs-mrs.fr

Abstract

Hydrogenases are efficient biological catalysts of H_2 oxidation and production. Most of them are inhibited by O_2 and a prerequisite for their use in biotechnological applications under air is to improve their oxygen-tolerance. We have previously shown that exchanging the residue at position 74 in the large subunit of the oxygen sensitive [NiFe] hydrogenase from *Desulfovibrio fructosovorans* could impact the reaction of the enzyme with O_2 (S. Dementin *et al*, J. Am. Chem. Soc. 131 10156-10164 2009; P. P. Liebgott *et al.*, Nat. Chem. Biol. 6 63-70 2010). This residue, a valine in the wild-type enzyme, located at the bottleneck of the gas channel near the active site, has here been exchanged with a cysteine. A thorough characterization using a combination of kinetic, spectroscopic (EPR, FTIR)~~, crystallographic~~ and electrochemical studies demonstrates that the V74C mutant has features of the naturally-occurring oxygen-tolerant membrane-bound hydrogenases (MBH). The mutant is functional during several minutes under O_2, has impaired H_2-production activity and has a weaker affinity for CO than the WT. Upon exposure to O_2, it is converted into the more easily reactivable inactive form, Ni-B, and this inactive state reactivates about 20 times faster than in the WT enzyme. Control experiments carried out with the V74S and V74N mutants ~~support this interpretation~~ indicate that protonation of the position 74 residue is not the reason the mutants reactivate faster then the WT enzyme. The electrochemical behaviour of the V74C mutant towards O_2 is intermediate between that of the WT enzyme from *Desulfovibrio fructosovorans* and the oxygen-tolerant MBH from *Aquifex aeolicus*.

1.Introduction

Dihydrogen is an energy carrier that constitutes a promising alternative to fossil fuels whose reserves are diminishing. Large scale use of H_2 will require overcoming several technological limitations relating to its storage, its clean production, and its efficient oxidation by cheap catalysts. Hydrogenases are very efficient biological catalysts of H_2 oxidation and production, and can be used in fuel cells to replace the standard noble-metal catalysts such as Pt or Pd[1,2]. By using hydrogenase-containing photosynthetic organisms (such as cyanobacteria or algae), it should be possible to convert solar energy into hydrogen using water as electron donor[3,4]. However, most hydrogenases are inactivated by dioxygen and this critically restricts their utilization to generate H_2 during photosynthesis. Thus, improving O_2-tolerance of these enzymes is a prerequisite for their utilisation in biotechnological processes.

Hydrogenases belong to either of three groups distinguished by the metal content of their active site: [NiFe], [FeFe] or [Fe][5]. The reaction of each of these enzymes with O_2 is different. Most [NiFe] enzymes are inactivated by oxygen[6] but their activity can be totally recovered after reduction. However, there are a few O_2-tolerant [NiFe] enzymes which are able to catalyse H_2-oxidation[7-9] or H_2-production under oxygen[10]. Identifying the molecular determinants that make some hydrogenases more tolerant to oxygen than others is pivotal in the perspective of using them in biotech processes.

The reactivity towards O_2 of the standard sensitive [NiFe] enzymes, purified from *Desulfovibrio gigas* (*Dg*), *D. vulgaris* (*Dv*), *D. fructosovorans* (*Df*) and *Allochromatium vinosum* (*Av*, formerly *Chromatium vinosum*), has been extensively studied. Upon exposure to air , these [NiFe] enzymes are converted into a mixture of two inactive states, Ni-A and Ni-B, that are differentiated by their EPR signatures and their reactivation rates under reductive conditions[6,11]. Ni-B reactivates in seconds while Ni-A requires several minutes or even hours. In these inactive states an oxygenated species bridges the active site Ni and Fe. Although the hydroxyl nature of this ligand in the Ni-B form is commonly accepted[6,12], the structure of the Ni-A state is still a mater of debate[12], and this complicates the studies of the inactivation mechanisms. According to current literature, the Ni-B state is generated in the presence of O_2 but also upon anaerobic oxidation of the enzyme. On the contrary, the Ni-A species is only formed by the reaction of O_2 at the active site. Based on crystallographic and spectroscopic studies of the sensitive *Df*, *Dv* and *Av* enzymes, it has been proposed that the Ni-A species houses a di-oxo bridging ligand (a μ-hydroperoxide) originating from the partial reduction of O_2 [13-15]. Nevertheless, a ^{17}O ENDOR study on the *Dg* enzyme showed that the oxygenic

bridge in Ni-A originates from solvent upon oxidation with air[16]. To solve the paradox, a reversible protonation and reduction of the hydroperoxide, using an electron provided by the reduced [3Fe-4S]-cluster, to a NiFe-bridging oxo species and a solvent exchangeable water molecule was proposed[13,14]. As reviewed in ref[12], the results of theoretical calculations suggest that the Ni-A state could also harbor a monooxygenic bridging ligand along with a sulfoxide or sulfenic acid ligand, which have been detected as partially occupied species in the crystal structures[13,15]. Some oxygen-tolerant [NiFe] enzymes have been described and the putative molecular determinants of their oxygen tolerance are different: restricted O_2-access to the active site in the case of the hydrogenase "sensors"[17-19], or presence of a Ni-coordinating selenocysteine instead of a cysteine, allowing H_2 production in the presence of O_2[10]. The oxygen tolerance of another group of membrane-bound [NiFe] hydrogenases [including the homologous membrane-bound hydrogenases from *Ralstonia eutropha* (*Re* MBH), hydrogenase I from *Aquifex aeolicus* (*Aa* MBH), and Hyd-1 from *E. coli* (*Ec* MBH)] results from the fact that they only convert into the Ni-B state under O_2[7,20]. Moreover, the reactivation rate of this inactive state is greater than that of the same species in oxygen-sensitive enzymes[21]. The reasons for this preferential conversion into a Ni-B form that reactivates rapidly are unknown. Contrary to their oxygen-sensitive counterparts[22], these MBH enzymes are nearly insensitive to CO inhibition[7,23,24] (a competitive inhibitor of standard hydrogenases) and they are poor catalysts of hydrogen production under reducing conditions[7,23,25].

We have previously shown that changing the side-chain of the residue at position 74 in the large subunit of the *Df* [NiFe] enzyme has an impact on the reaction of the enzyme with O_2[19,26]. This residue is located at the bottleneck of the gas channel in the vicinity of the active site (Fig 1). Here we report the effect of the V74C mutation which results in a phenotype similar to that of the above-mentioned resistant MBH enzymes. The mutant is active for hydrogen oxidation but its hydrogen production activity is impaired, and it is also less inhibited by CO than the WT. Moreover, under conditions where aerobic inactivation of the WT enzyme produces mainly the Ni-A state, V74C is only converted into the Ni-B form. This inactive form is identical to that observed with the WT enzyme from a spectroscopic and thermodynamic point of view but it reactivates much faster. In control experiments, we show that the V74S and V74N mutations also accelerate, to a lesser extent, the reactivation of the anaerobically formed inactive state. We propose that the V74C mutant is preferentially converted into the Ni-B form that quickly reactivates because C74 accelerates the electron

transfer to the active site in the presence of O_2. Interestingly, this mutant was not designed in an attempt to copy the sequences of the above-mentioned resistant enzymes.

2. Materials and Methods

2.1. Preparation of the hydrogenases. The *Df* hydrogenase mutants were constructed using the bacterial strains, plasmids, growth conditions, site-directed mutagenesis strategy and the enzyme purification protocol as described in ref[19,27]. The purification yield of the recombinant V74C, V74S and V74N mutants, about 1 mg per liter of culture, is similar to that of the WT enzyme. The qualification "as-prepared" refers to enzymes purified under aerobic conditions, and not yet reductively activated. Several activation procedures can be used: incubation for hours under H_2 (for preparing EPR and FTIR samples), electrochemical reduction (in PFV and FTIR experiments) or chemical reduction with dithionite and/or reduced methyl viologen (before performing solution assays of the activity or for preparing reduced EPR samples).

The *Aa* enzyme was purified as described in ref[7].

2.2. Kinetic characterization. The H_2-oxidation activity of the *Df* enzymes was assayed with methyl viologen (MV) as electron acceptor as previously described[27].

The hydrogen/deuterium exchange (HDE) activity of the *Df* enzymes was assayed by membrane-inlet mass-spectrometry to measure the rates of H_2 and HD production in solution, in the presence of D_2; it is expressed in $\mu mol.min^{-1}.mg\ protein^{-1}$, see ref[28] for details. The effect of O_2 on HDE activity was monitored by adding a defined volume of air-saturated water during the assay as already described[26].

Protein film electrochemistry experiments (cyclic voltammetry and chronoamperometry) were carried out in a glovebox filled with N_2, using the electrochemical setup and equipment previously described[19]. The two-compartment electrochemical cell was kept at the desired temperature value using a water circulation system. The rotating pyrolytic graphite edge working electrode (PGE) (area $A \approx 3\ mm^2$) was used in conjunction with an electrode rotator, a platinum wire was used as a counter electrode, and a saturated calomel electrode (SCE), located in a side arm containing 0.1 M NaCl and maintained at room temperature, was used as a reference. All potentials are quoted versus the standard hydrogen electrode (SHE), ($E^{SHE} = E^{SCE} + 240$ mV). The electrochemical cell contained a buffer mixture of MES, CHES, TAPS, HEPES and sodium acetate (5 mM each) and 0.1 M NaCl; the temperature (T) and pH are indicated in each caption. The protein films were prepared by painting the electrode with

about half a microliter of a stock enzyme solution (about 10 μM of enzyme in the mixed buffer at pH 4.0). The enzyme-coated electrode was inserted in the electrochemical cell containing the buffer mixture at pH 5.5, 40 °C, under an atmosphere of H_2. The enzyme films were fully activated by poising the rotating electrode at -560mV under 1 atm of H_2, for 1-10 minutes, until the hydrogen oxidation current measured at -160mV stabilized.

The Michaelis constant was determined as previously explained[19] by measuring the decrease in H_2 oxidation current (at pH 7, -160 mV) while H_2 is flushed from the cell solution by a stream of Argon. We employed the methods described in ref[19,22] to determine the kinetics of inhibition by CO. The activity is measured at a fixed potential (-160mV, pH 7), while small aliquots of a buffer, saturated with pure CO at 40°C and kept in a capped serum bottle, are injected with gastight syringes into the cell solution, which is continuously flushed with H_2.

In experiments aimed at measuring the rate of reactivation of the enzyme by monitoring the increase in H_2 oxidation current at -90mV vs SHE, pH 5.5, after the enzyme had been inactivated (Fig 5), three distinct inactivation procedures were tested. Procedure A (supplementary Fig S4A) consisted in inactivating the enzyme under anaerobic conditions by stepping the electrode potential at +215mV for 1500s, followed by a step to -90mV to drive reactivation. Such anaerobic inactivation under H_2 forces the formation of the Ni-B state[29]. Procedure B (supplementary Fig S4B) consisted in monitoring the H_2 oxidation current under 1 atm of H_2 at -90mV for 400s, then step the potential to +90mV (still under H_2) and immediately inject 0.1 mM O_2; oxygen is progressively flushed from the cell by the stream of H_2 for 200s before stepping the potential to -90mV to drive reactivation. This aerobic inactivation under H_2 at relatively low electrode potential is known to result in the formation of the Ni-B inactive state in the *Av* [NiFe] hydrogenase[20]. Procedure C (supplementary Fig S4C) consisted in monitoring the H_2 oxidation current under 1 atm of H_2 at -90mV for 200s, then monitoring the H_2 production current at -560mV for 400s under 1 atm of Argon, then stepping the potential to +215mV (still under Argon) and immediately injecting 0.1 mM O_2 using a stock solution of buffer saturated with pure O_2. Oxygen is flushed from the cell by the stream of Ar, and H_2 is reintroduced 60s before stepping the potential to -90mV to drive reactivation. Such aerobic inactivation under Argon at relatively high electrode potential is known to result in the formation of the Ni-A inactive state in the case of the [NiFe] hydrogenase from *Av*[20]. In all cases, before analyzing the reactivation kinetics, we eliminated the contribution of the capacitive current by subtracting the current recorded in a control experiment where a bare electrode (no enzyme adsorbed) was subjected to the same series of potential steps.

We used the following equations to determine the rates of the reactivation processes from the current against time kinetic traces.

First order reactivations could be fitted to

$$i = i_\infty[1 - \alpha_{\text{fast}} \exp(-t/\tau_{\text{fast}})] \exp(-t/\tau_{\text{film}}) \quad (1)$$

by adjusting the four following parameters: i_∞ is the current that would be reached after the reactivation if there were no film loss, τ_{fast} is the time constant of reactivation, α_{fast} is the initial fraction of inactive enzyme, and τ_{film} is the time constant of film loss[30].

When two distinct species reactivate at two different rates, the equation that describes the increase in current is

$$i = i_\infty[1 - \alpha_{\text{fast}} \exp(-t/\tau_{\text{fast}}) - \alpha_{\text{slow}} \exp(-t/\tau_{\text{slow}})] \exp(-t/\tau_{\text{film}}) \quad (2)$$

However, the 6 parameters in equation (2) cannot be independently determined if $t \ll \tau_{\text{slow}}$ (that is if the slowest phase is slower than the time scale of the experiment). Indeed, equation (2) then reduces to

$$i = i_\infty[1 - \alpha_{\text{slow}} + \alpha_{\text{slow}} t/\tau_{\text{slow}} - \alpha_{\text{fast}} \exp(-t/\tau_{\text{fast}})] \exp(-t/\tau_{\text{film}}) \quad (3)$$

which depends on only 5 independent parameters: $i_\infty(1 - \alpha_{\text{slow}})$, $i_\infty \alpha_{\text{fast}}$ (these two parameters may not be equal if the enzyme is not fully inactivated when the reactivation begins), $i_\infty \alpha_{\text{slow}}/\tau_{\text{slow}}$, τ_{fast} and τ_{film}. Therefore, when the reactivation shows a slow phase, the time constant and the amplitude of this slow phase cannot be independently determined by simply fitting the reactivation trace.

To determine the time constant of anaerobic inactivation, the change in current after a step potential, the inactivation trace (dashed line in Fig 8) was fitted to an equation that is analogous to equation (1):

$$i = [(i_0 - i_\infty) \exp(-t/\tau_{\text{fast}}) + i_\infty] \exp(-t/\tau_{\text{film}}) \quad (4)$$

Note that if i_∞ is small (that is, if the inhibition is irreversible), τ_{fast} and τ_{film} cannot be independently determined.

We analyzed the electrochemical data using "SOAS"[31] , an open-source program available on our web site at http://bip.cnrs-mrs.fr/bip06/software.html.

2.3. EPR spectroscopy. EPR spectra were recorded on a Bruker ELEXSYS 500E spectrometer fitted with an Oxford Instruments ESR 900 helium flow cryostat[32]. Redox titrations were performed in an anaerobic cell as described previously[32]. For Ni-C into Ni-L photoconversion studies, the sample was illuminated directly in the EPR cavity through a

fiber optic by using a 250 W (Fiberoptic-Heim) quartz lamp. Kinetics of the Ni-L2 into Ni-C recombination process was determined as follows: at a given temperature, the sample showing the Ni-C signal was irradiated to generate the Ni-L2 state then the irradiation was turned off and the decay of the Ni-L2 signal (or the growth of the Ni-C state) was measured as a function of time in the dark[26]. All the potentials are given *vs* SHE.

2.4. FTIR spectroscopy. The infrared experiments were done in a spectroelectrochemical cell (activation and anaerobic inactivation)[33] or in a gas-tight transmission cell (aerobic inactivation)[34]. In the case of aerobic inactivation experiments, the O_2 concentration varies from 0 to 200µM. All the potentials are given *vs* SHE.

3. Results

3.1 Kinetic properties of V74C: Michaelis parameters in H_2-oxidation and inhibition by CO. The properties of V74C were determined by different assays. We found that, after activation under reducing conditions, its H_2-oxidation activity with 50 mM methyl viologen (MV) under 1 atm H_2 (700 s^{-1}) is comparable with that of the WT enzyme (750 s^{-1})[27]. The apparent affinity of the V74C mutant for H_2 determined by PFV is greatly affected ($K_m(H_2)$ = 610 ± 320 matm H_2 compared to 10 ± 5 matm H_2 for WT). This value was used to calculate the catalytic constant under infinite concentration of H_2 using the Michaelis-Menten equation: the k_{cat} of V74C is 1050 ± 260 s^{-1}, a value in the range of that of the WT enzyme (760 ± 95 s^{-1}). H/D exchange rate was decreased in the mutant (10 µmol/min/mg in V74C after 2 min of activation with reduced MV in the measurement vessel *vs* 50 µmol/min/mg in WT). The value of k_{out}/k for hydrogen, determined following the methodology described in ref[27], was slightly smaller in the mutant: 0.75 *vs* 1.75. This indicates a slight decrease in gas diffusion rate within the enzyme, which might contribute to the decrease in exchange rate. The rate constants for binding and release of CO (a competitive inhibitor with respect to H_2) were determined by PFV and corrected by using the value of $K_m(H_2)$ to take into account the protective effect of the substrate[22,27]. We found that, at 9°C, the corrected rate constant for CO binding ($k_{in}(CO)$=120±50 s^{-1}.matm$(CO)^{-1}$) of V74C is approximately 10 times slower than that of the WT while the true rate constant for CO release ($k_{out}(CO)$=1.5±0.5 s^{-1}) is similar. Thus the CO-inhibition constant ($K_i(CO)$) is 0.0125 matm(CO) (this value is 25 times higher than that of WT). At 40°C, the rate constants of CO binding and release are too fast to be

measured, but we also found that the corrected inhibition constant is about 20 times greater in V74C than in the WT (20 *vs* 1 matm(CO)).

3.2 HDE activity of V74C under O_2. The tolerance of the active site to O_2 was tested by performing the HDE in the presence of a controlled concentration of O_2, as described in Dementin *et al.*[26]. Whereas the WT enzyme is inhibited in seconds in the presence of 5 to 10µM O_2, the V74C mutant is more tolerant. ~~and is able~~ The ability of the V74C's active site to oxidise D_2 in the presence of such O_2 concentrations is demonstrated by the consumption of all the ~~injected~~ oxygen that has been injected (Fig 2). ~~Supplementary figure 1 reports the residual hydrogenase activity in function of [O_2].~~ This oxygen consumption is mediated by reduced MV, which is produced through hydrogen oxidation by the enzyme; during this time period, the catalytic activity of the enzyme being coupled with electron transfer, H/D recombination at the active site does not occur and HDE is therefore inhibited. Supplementary figure 1 reports the residual hydrogenase activity ~~in~~ as a function of [O_2]. The consumption of O_2 intensifies the protective effect of the mutation since O_2 is only temporarily present. When oxygen is totally depleted the mutant starts again catalyzing the standard HDE reaction. This sequence of O_2 consumption in presence of MV and recovery of HDE activity after O_2 depletion is reminiscent of the behaviour of the previously characterized O_2-tolerant V74M and V74M/L122M mutants (fig 2 in ref [26]). It may be interesting in the future to determine whether this oxygen reduction activity also accurs with cytochrome c3 as electron shuttle, and to test the behaviour of a strain of *D. fructosovorans* producing V74C upon exposure to O_2; this is out of the scope of this paper

3.3 Spectroscopic and structural characterization of as-prepared and reduced V74C. EPR spectroscopy was used to study the impact of the cysteine at position 74 on the magnetic properties of the active site. In the as-prepared WT enzyme, the paramagnetic Ni gives rise to the Ni-A and Ni-B signals (Fig 3A). They correspond to 20-80% of total Ni, depending on the enzyme preparation[26]. The ratio of Ni-B over Ni-A strongly varies between preparations[26]. In the five V74C preparations we examined, the Ni-Fe center was mostly EPR silent, the Ni signals never exceeding 0.2 spin/molecule in the as-prepared state. This paramagnetic Ni comprises the two standard Ni-A and Ni-B signatures whose ratio Ni-B/Ni-A greatly varies, as observed in WT enzyme (Fig 3a). The reduction potentials of Ni-A/Ni-SU and Ni-B/Ni-SI couples determined at pH 8.0 upon stepwise reduction with dithionite and reoxidation with ferricyanide are slightly higher than those of the WT enzyme (-130 ± 20 mV and -145 ± 20

mV for Ni-A/Ni-SU and Ni-B/Ni-SI, respectively; supplementary Fig S2; the Ni-A/Ni-SU and Ni-B/Ni-SI redox potential for WT enzyme determined at pH 8.0 are -160 ± 20 mV). The paramagnetic Ni also comprises a new rhombic signal at g=2.11, 2.10, 2.01, which accounts for 0.01-0.07 spin per molecule, depending on the preparation (Fig 3b and e) and which is redox-reversible. Upon reduction with dithionite or H_2, the three signatures vanish and the standard Ni-C signal appears. This signature is typical of the reduced form of the WT enzyme[6] and represents up to 50% of total Ni, depending on the reductive treatment (Fig 3d and e). This demonstrates that a large part of the oxidized Ni-silent species is converted into a standard reduced form upon reduction. At 6K, the split Ni-C signal displays the same characteristic pattern due to magnetic interaction with the reduced proximal $[4Fe\text{-}4S]^{+}$, as in the WT enzyme[41] showing that neither the relative arrangement nor the exchange coupling between these two centers are modified by the mutation (data not shown).

The Ni-C state of the V74C keeps the well-known property of light-sensitivity which is reversible upon annealing of the sample[12,42,43]. The rate constants of the recombination of Ni-L_2 into Ni-C were measured between 130 and 150K. In the V74C, the kinetics of recombination followed a mono-exponential decay as observed for the WT and the corresponding first-order rate constant was accelerated by a factor 2, whereas the activation energy of the process was the same in the two enzymes (30 ± 3 $kJ.mol^{-1}$ for V74C *vs* 36 ± 3 $kJ.mol^{-1}$ for WT). This light-sensitivity, that is interpreted in terms of photo-induced proton transfers in the coordination of the Ni ion, is probably intimately linked to the ability of the active site to exchange protons with its close environment[43]. These observations then suggest that only small modifications of the H-bond network are likely to occur near the active site in the mutant.

The spectral contributions of Fe-S clusters in both oxidized and reduced samples showed no difference with the WT enzyme (data not shown). The redox potential of the $[3Fe\text{-}4S]^{+}/[3Fe\text{-}4S]^{0}$ transition was determined in the mutant to be +0 mV ± 20 mV at pH 8.0. This is in the range of the value measured for WT (+65 mV)[44] and closer to those determined in the homologous enzymes from *D. gigas* and *D. vulgaris*[45]. At low potential, the number of data points of the titration was not sufficient to determine the redox potentials of the $[4Fe\text{-}4S]^{2+/1+}$, but their signals developed in the same potential range as observed in the WT.

The diatomic ligands CO and CN^{-} of active site Fe atom also provide a spectroscopic signature of the active site: they are detected by IR spectroscopy in the 1900-2100 cm^{-1} region. Each redox state of the active site is defined by a set of three IR bands (1 CO and 2 CN^{-} ligands)[6] whose frequencies depend on the redox state of the active site. The

spectra obtained for the as-prepared samples of V74C and WT enzymes at pH 8.0 show significant differences. In the latter, a mixture of Ni-A and Ni-B forms is generally observed (Fig 4Aa). In the Ni-A state the enzyme shows an intense band at 1947 cm^{-1} corresponding to the stretching vibrational mode of the CO ligand and two less intense bands at 2096 and 2084 cm^{-1} due to the two CN^- ligands. In the Ni-B state, the CO and the two CN^- ligands give rise to bands at 1946, 2080 and 2091 cm^{-1}, respectively[33]. The CO bands of the Ni-A and Ni-B states overlap, showing a single peak because the spectral resolution is 2 cm^{-1} (Fig 4Aa). The spectrum of the V74C mutant is more complex and suggests a mixture of different, unprecedented active sites structures (Fig 4Bg), ~~consistent with the X-ray (see below)~~. It shows three CO bands at 1960, 1954 and 1943 cm^{-1}. The corresponding six CN^- bands probably overlap with two main peaks at 2078 and 2087 cm^{-1} emerging. In addition, the CO and CN^- bands corresponding to the standard Ni-A state are observed but the bands related to the Ni-B state are not resolved.

An electrochemical titration allowed the determination of the half-reduction potentials of the Ni-A/Ni-SU and Ni-B/Ni-SI conversion processes in the WT enzyme (E'= -195 mV and -175 mV at pH 8.0, respectively[46]). A spectrum obtained at -280 mV is shown in Fig 4Ab. The corresponding redox titration of as-prepared V74C at 5°C, pH 8.0 was also performed. The spectrum obtained at -305 mV is shown in Fig 4Bh. The Ni-A bands disappear to yield the Ni-SU bands, as occurs with the WT enzyme. The Ni-SU CO band is detected at 1949 cm^{-1} (as in the WT) but, surprisingly, the two Ni-SU CN^- bands are shifted 16-17 cm^{-1} towards lower frequencies. We thus propose to call this state Ni-SU'. The reductive conversion of the CO band of Ni-A (1947 cm^{-1}) into the Ni-SU' one (1949 cm^{-1}) fits best to a mono-electronic process (E'= -175 ± 15 mV, 20 mV higher than that described for the WT's Ni-A to Ni-SU conversion, see additional Fig 2A). Both the 1960 and 1954 cm^{-1} CO-bands disappear simultaneously to yield a band pattern similar to that of the Ni-R_{II} state of WT, according to a bi-electronic Nernstian process with E'= -180 ± 5 mV (additional Fig 2B). The CO band at 1942 cm^{-1}, still detected at -305 mV (Fig 4Bh), is converted at lower potential into the Ni-R states. After as-prepared WT and V74C are poised at low potential for a long time (-295 mV for 210 min and -555 mV for 180 min, respectively) for activation of the active site, only the Ni-R_I and Ni-R_{II} states are detected at potentials below -480 mV (Fig 4Ac and Fig 4Bi).

In summary, the aerobically prepared V74C mutant is present as a mixture of several novel inactive forms (one of which probably being EPR-detectable) which may be activated by reduction or H_2 to yield the standard active forms observed for the WT enzyme.

In addition, a minor fraction of the as-prepared enzyme is in the standard Ni-A/Ni-B states whose thermodynamic properties are similar to those of the same species in the WT enzyme.

3.4 Anaerobic inactivation and reductive reactivation of V74C followed by FTIR-electrochemistry and PFV. Anaerobic formation of the inactive Ni-B state occurs in the presence of chemical oxidant like DCIP[47] or at high electrode potential[29,48]. FTIR-electrochemistry was used to study the anaerobic inactivation of the V74C mutant. After activation under prolonged H_2-incubation or poise for a few hours at -554 mV in the presence of a cocktail of mediators, V74C in the reduced state was subjected to stepwise oxidation (Fig 4). As observed for the WT enzyme, upon increasing the potential, the Ni-R bands are converted into the Ni-C (Fig 4Bj), then Ni-SI (Fig 4Bk) and finally Ni-B (Fig 4Bi) bands. As a control, the process is shown for the WT enzyme in Fig 4Ad,e,f. The formal potentials measured for the V74C Ni-SI/Ni-C and Ni-C/Ni-R couples are approximately -370 mV and -450 mV, respectively, at pH 8.0 and 25ºC (see supplementary Fig S3). These values are in the range of those measured with the WT enzyme[46]. The titration of the Ni-B/Ni-SI couple is well described by a one-electron Nernstian process with E'=-135±10 mV (supplementary Fig S3). This is slightly higher than the value measured for the WT enzyme (E'=-175 mV[46]) and consistent with the titration followed by EPR (supplementary Fig S2).

Interestingly, the Ni-SI to Ni-B conversion, driven by stepping the potential from -255 mV to -4 mV, is so fast at 25°C that we had to perform the experiment at 5°C to accurately determine the reaction rate. At this temperature, the first-order rate constant of the Ni-SI/Ni-B conversion (0.067 min^{-1} ± 0.007) is 16 times higher than that of WT enzyme (data not shown). We used PFV to measure the reactivation rate of the WT and V74C enzymes after anaerobic inactivation at high potential under H_2 (procedure A, described in the Material and Methods section and supplementary Fig S4A). In the case of the *Av* [NiFe] hydrogenase, this drives the formation of the Ni-B "ready" inactive state[29]. The electrode potential was then stepped to –90 mV to drive activation. The activation of V74C is monophasic and occurs with a first order rate of about 0.5 s^{-1} (time constant: 2 s) (purple trace in Fig 5A). Under the same conditions, which are expected to favour the formation of the Ni-B species; the reactivation of the WT enzyme is dominated by a much slower fast phase (0.028 s^{-1}, time constant: 36 s). Fourmond *et al.*[48] showed that the value of E_{switch} (the potential where reductive reactivation occurs, in voltammograms recorded at slow scan rate, see fig 6) depends on the logarithm of the ratio of rate of activation over scan rate: the greater E_{switch} at a given scan rate, the faster the reactivation at a given potential. Fig 6 shows that the E_{switch} of V74C (+35 ± 5 mV) is about

130 mV more positive than that of WT (-90 ± 10 mV). This is consistent with the observation in fig 5A than Ni-B reactivates much more quickly in the mutant.

In summary, the FTIR-electrochemistry and PFV data show that upon anaerobic inactivation the WT and mutant enzymes are converted into the standard Ni-B form. However, the reductive reactivation rate of this form is much faster in the case of the V74C mutant.

3.5 Aerobic inactivation and reductive activation of V74C after O_2 attack. Figure 7 shows the FTIR spectrum of the H_2-activated WT and V74C enzymes reoxidized with air. The WT spectrum is a mixture of Ni-A, Ni-B and another unidentified, EPR silent state. This unidentified state with a 1911 cm^{-1} CO band and two corresponding CN^- bands at 2059 and 2068 cm^{-1} is different from the Ni-SI_I whose CO and CN^- frequencies are 1913, 2054 and 2069 cm^{-1}, respectively (see Fig 4e). The amount of this species changes from one preparation to another; for example it is not detected in the sample whose as-prepared state spectrum is shown in Fig 4Aa. A similar state in which a sulphide was proposed to bridge both metals of the active site has been described for the as-prepared *Av* enzyme and was shown to be EPR-silent[49]. The spectrum of as-prepared V74C is similar to that shown in Fig 4Bg.

After 4 hours under H_2, we detect the Ni-R_I and Ni-R_{II} states in both enzymes (like after electrochemical reduction, Fig 4Ac and Fig 4Bi). Beside, a 1907-1909 cm^{-1} CO band appears upon reduction of the 1911 cm^{-1} band in the WT sample (Fig 7Ab), as described for the *Av* enzyme[49]. This signal decreases during activation. Reoxidation of the WT by removing the septum of the vial and exposing the sample to air leads to a mixture of bands corresponding to 33% Ni-A, 48% Ni-B and 19% of the above-mentioned unidentified state as estimated by Fourier deconvolution of the FTIR spectrum. Under identical conditions, V74C is immediately converted to the Ni-B state only. The bands detected in the as-prepared V74C mutant are no longer detected (Fig 7Be).

The inhibition by O_2 is easily assessed by PFV because O_2 does not interfere with the electrochemical measurement of activity, provided that the electrode potential is high enough that O_2 is not reduced on the electrode. The continuous lines in Fig 8B show the current recorded with the WT (red) and V74C (purple) enzymes, when the potential of the rotating electrode is poised at +140 mV and small aliquots of a solution saturated with air are injected in the electrochemical cell which is continuously flushed with H_2 (as shown in Fig 8A). These currents were recorded after a 200s (WT) or 500s (V74C) poise at +140 mV; in the case of the mutant, the anaerobic inactivation at + 140 mV is also shown as a dashed purple line in Fig

8C. Three aliquots of 100, 200 and 500 µL of an air-saturated buffer solution (4, 8 and 20 µM of O_2, respectively) have been injected. Figure 8A shows that the concentration of O_2 in the cell increases immediately after each injection and then drops back to zero in less than one minute because the cell is continuously flushed with H_2[22]. The mutant spontaneously reactivates whereas the WT enzyme reacts irreversibly with O_2 under such oxidative conditions (of course the fast reactivation of both enzymes can be driven by taking the electrode potential down, as seen in Fig 5). The rate of reactivation of the V74C enzyme can be estimated by simply fitting the reactivation phases to an exponential function (Fig 8D); this returns time constants in the range 100-140s, which are about ten times higher than the time constant for the decrease of the oxygen concentration after the injection[22]. Therefore, the reactivation is not limited by O_2 exhaustion from the cell solution, but rather by the rate of anaerobic equilibration between inactive and active species. This was confirmed by comparing the rate of reactivation after O_2 had been flushed out and the rate of inactivation at the same potential before O_2 was added: fitting the purple line in Fig 8C to eq (4) (dashed black line) returns a time constant of 140s. The fact that, at a given potential, the time constant of anaerobic inactivation is the same as the time constant of reactivation after aerobic inhibition shows that the reaction with O_2 forms the same inactive species as that formed under anaerobic conditions: this was also observed with the oxygen resistant *Aa* [NiFe] hydrogenase (see the discussion of Fig 6 in ref[7]).

To confirm that both aerobic and anaerobic inactivations of the V74C mutant produce the Ni-B state irrespective of the inactivation procedure, we analyzed the kinetics of reactivation at -90mV after inactivation under various conditions. Aerobic inactivation under H_2 at moderately high potential (+90mV, procedure B) produces mainly the Ni-B state in the case of *Av*[20] [NiFe] hydrogenase. Figure 5B shows that the reactivation of the V74C and WT enzymes inactivated under these conditions is indeed the same as that after anaerobic inactivation (panel A).

The activation that follows the aerobic inactivation of the enzymes under argon at very high potential (+215mV) is shown in Fig 5C. This inactivation procedure, which is called "C" in the Materials and Methods, was shown to result in the formation of Ni-A in the [NiFe] hydrogenase from *Av*. Indeed, the subsequent reactivation of the WT is clearly biphasic, and dominated by a slow phase (slower than 1000s) whose rate cannot be determined (cf the discussion of eq (2-3)). In contrast, the reactivation of the V74C mutant is essentially monophasic and has a time constant of about 2s (purple line in Fig 5C).

Therefore, the reactivation of the V74C mutant is fast and follows first order kinetics irrespective of the inactivation procedure, showing that the mutation prevents the formation of the Ni-A state upon reaction with O_2. Moreover, all things being equal, the Ni-B state reactivates about 20 times faster in the V74C mutant than in the WT. Taken together, the FTIR-electrochemistry and PFV experiments suggest that the V74C mutant inactivated by O_2 is converted only into the Ni-B form. The spectroscopic properties of this form are identical to those of WT but it reactivates much faster.

3.6 Impaired H_2-production activity of V74C. The red voltammogram in Fig 6 show that the WT enzyme can catalyze both H_2 oxidation (positive current) under oxidizing conditions and H_2 production (negative current) at low electrode potential (even in the presence of 1 atm of H_2, which inhibits proton reduction[22,50]). In contrast, the voltammogram of V74C (purple line in fig 6) shows no detectable proton reduction activity at low potential. The experiment in supplementary Fig S4C also shows that the ratio of H_2 production rate in the absence of H_2 over H_2 oxidation rate is close to 1 for the WT enzyme and much smaller for the mutant: in these experiments, the H_2 oxidation currents observed with the two enzymes at -90mV, under 1 atm of H_2 (between t=0 and 200s) are similar, whereas the magnitude of the H_2-production current at -560mV (between t=200 and 600s) is much smaller with the V74C mutant than with WT. Thus V74C is biased towards H_2-oxidation.

3.7 Comparison with the *Df* V74S and V74N mutants. To further address the role of cysteine 74 in modulating oxygen tolerance, we constructed the V74S and V74N mutants. In the absence of crystal structures, we may hypothesise that the alcohol group of S74 takes the same position as the thiol group of C74, whereas in the V74N mutant, the amide group is likely to introduce a steric constraint. The pKas of an alcohol and an amide being several pH units higher and lower, respectively, than that of the corresponding thiol, the side chains of N74 and S74 are very unlikely to mediate proton transfer, and therefore comparing the properties of the V74C and V74S/N mutants should inform on whether proton transfer on the side chain of the position 74 residue is essential in increasing oxygen tolerance.

The specific activities of V74S and V74N in solution assay with MV are 375 s^{-1} and 640 s^{-1} respectively. Upon exposure to oxygen under the conditions used in Fig 8 (+140 mV, 1 atm H_2), the V74S and V74N mutants spontaneously reactivate (cf the increase in current seen on the cyan and green traces at 200s, 600s and 1100s) but with a slower rate and smaller magnitude than for V74C (purple trace). Figure 5A shows that the V74S and V74N mutations

also significantly increase the rate of reactivation after inactivation under anaerobic conditions (0.11 and 0.3 s^{-1} respectively, compared to 0.028 s^{-1} for the WT), although these rates are smaller than that of V74C (0.5 s^{-1}). Clearly, the rate of reactivation after anaerobic inactivation does not correlate with the pKa of the position 74 amino acid side chain.

3.8 Comparison with the *Aa* MBH. We compared the reactions with O_2 of the *Df* enzymes and the oxygen tolerant *Aa* MBH. The dark blue trace in Fig 8 shows that at +140 mV under H_2 the *Aa* enzyme is quickly inhibited after each injection but reactivates faster than the *Df* enzymes. It is striking the behaviour of V74C (purple trace) is intermediate between the *Df* WT and *Aa* WT enzymes. The *Aa* enzyme has little H_2 production activity (Fig 6)[7] and is converted only into the Ni-B state upon O_2 attack[7]. However, it has been shown that the Ni-A state can be obtained in the *Aa* enzyme upon O_2 exposure at high temperature (85°C), this indicates that in this enzyme the Ni-B formation is kinetically favoured[51]. The reactivation rate of this species is too fast to be determined under the conditions of Fig 5A (+90 mV, 40°C, pH 5.5, 1 bar H_2) but could be estimated to 30 s^{-1} from extrapolating the data from Fig 4 in ref[48] (+90 mV, 40°C, pH 6, 1 bar H_2).

4. Discussion

The oxygen sensitivity of most hydrogenases limits their use in bioprocesses in which H_2 is oxidized or produced. The use of naturally-occurring oxygen-resistant enzymes can overcome this restriction and molecular devices using them to produce electricity[52] or to convert light energy into H_2[53-55] show promising results. Another strategy consists in engineering hydrogenases of interest. This is practically inevitable when one wants to exploit the hydrogen metabolism of some phyla (including Cyanobacteria, which possess a [NiFe] hydrogenase whose catalytic subunit is homologous to that of the *Df* enzyme). As the heterologous expression of [NiFe] hydrogenases is difficult because of their complex and host-specific maturation process, improving the oxygen tolerance of the endogenous enzymes seems to be a more viable option. In this respect, understanding how resistant proteins manage to tolerate O_2 can be inspirational. In the sensor hydrogenases (RH from *Re* and *Rhodobacter sphaeroides*), two bulky residues (Phe and Ile) at the entrance of the active site were proposed to restrict the O_2 access[17,18,35]. However, strictly copying the active site entrance of the sensor enzymes, by replacing the two corresponding residues V74 and L122 by Ile and Phe, respectively, in the *Df* enzyme is not sufficient: the V74I/L122F mutation

does not slow down O_2 diffusion to the point of decreasing the overall oxygen inhibition rate[19]. In contrast, the same mutant of the *Re* MBH enzyme (V77I/L122F) is apparently *less* O_2-tolerant than the WT enzyme: its apparent O_2 inhibition constant is decreased about 4-fold[56]. On the basis of primary structure comparisons, Ludwig *et al.*[56] proposed that the active site environment of the [NiFe] Re MBH and enzymes from the *Desulfovibrio* genus are nearly identical. Only Y77 and V78 of the *Df* enzyme are replaced by G80 and C81 in the *Re* enzyme. Mutants at the G80 position could not be purified because of instability. The C81A/S/T/V MBH mutants are not particularly oxygen sensitive[56]. We constructed and purified the Y77G/V78C mutant of the *Df* enzyme in an attempt to reproduce the environment of the MBH enzyme, but this did not decrease the rate of inhibition by O_2 of the enzyme[57]. There is evidence that replacing two cysteines near the proximal 4Fe4S cluster of the Re MBH enzyme with glycine makes the enzyme oxygen sensitive[58], but we failed to characterize the effect of the reverse mutation in *D. fructosovorans*, because the double cysteine mutant does not fold (unpublished results of ours).

We obtained unexpected and promising results without trying to copy the sequence of the oxygen-tolerant enzymes. With a Met or a Gln at position 74 in the *Df* enzyme, the slow diffusion of O_2 along the gas channel limits the rate of the inhibition reaction[19]. This resulted in mutants being inhibited by oxygen up to 10 times more slowly than the WT enzyme. Moreover, we showed that the V74M mutant was able to keep a prolonged activity under O_2. The X-ray structure of this mutant showed that the tolerance is not related to the oxidation of the methionines; instead it probably results from a slowed diffusion of O_2 through the gas channel and a facilitated, sulphur-assisted reactivation of the Ni-A inactive state[26].

Since we noticed that changing the amino acid at position 74 can affect the enzyme's reactivity towards O_2, we examined the effect of a thiol at this position. Air-purified V74C displays spectroscopic features different from WT. New FTIR signatures (mostly EPR-silent) ~~indicating~~ suggest that the active site of V74C is a mixture of states structurally different from the classical as-prepared states of WT. A small but significant fraction of the unready Ni-A/Ni-B (up to 20% enzyme molecules) states is nevertheless detected. Upon reduction, V74C in the as-prepared state is converted into the standard activated forms observed with the WT enzyme (Ni-SI, Ni-C, Ni-R). This strongly suggests that, after activation, the two enzymes have, apart from the mutated residue, essentially identical active site structures. A ~~significant~~ structural reorganisation in the V74C mutant is required to recover the standard WT-like activated structure. Once activated, the V74C mutant could not be converted back to the as-

prepared state by either anaerobic or aerobic oxidation following the procedures we described for the FTIR and PFV experiments.

Comparing the reaction with O_2 of this mutant with the *Df* and *Aa* WT enzymes (Fig 8) we observe that its properties are intermediate between the WT enzyme and the enzyme from *Aquifex aeolicus*, which is a prototype of oxygen tolerant enzyme[7,48]. It is also clear that the V74C mutant exhibits a number of properties that are usually the landmarks of oxygen-resistant MBH:

(i) The "catalytic bias" of hydrogenase, defined as the ratio of the rates of oxidation of H_2 under oxidative conditions and production of H_2 under reductive conditions[10,59], is easily assessed in a single PFV experiment. We observed (Fig 7 and supplementary Fig S4C) that like *Aa* hydrogenase[7] and unlike WT *Df* hydrogenase, the V74C mutant is active for H_2 oxidation but has very little H_2 production activity.

(ii) V74C has a weaker affinity for the competitive inhibitor CO, its K_i(CO) is 20-25 times higher than that of WT.

(iii) The V74C mutant is oxygen-tolerant. The PFV experiments demonstrate that in the presence of H_2, at a potential where WT enzyme is quickly inhibited and only reactivable by reduction, V74C is reversibly inhibited by O_2 (Fig 8), and spontaneously reactivates without reductive treatment when O_2 is removed from the cell solution. In addition, the HDE experiments show that, contrary to WT, V74C catalyses H_2 oxidation under O_2 (Fig 2). The progressive MV-mediated reduction of oxygen upon catalytic oxidation of D_2 (or H_2) is possible only if the enzyme functions in the presence of O_2. The reduction of O_2 is complete when its initial concentration is lower than 30 µM in the conditions of the assays. Above this concentration, the mutant enzyme is fully inhibited before O_2 exhaustion is complete.

(iv) Upon aerobic inactivation, V74C is converted into a Ni-B form that reactivates faster than in the WT:

The FTIR experiments in Fig 7 show that, upon reaction with O_2, the mutant is only converted into the Ni-B form whereas the WT is transformed into a mixture of Ni-A and Ni-B. The Ni-B form of V74C has the same thermodynamic and spectroscopic properties as the same species in the WT (Figs 3 and 4, and supplementary Figs S2 and S3). Moreover, the PFV experiments show that the mutant inactivated under either anaerobic or aerobic conditions reactivates at the same rate, supporting the idea that irrespective of the inactivation conditions, the inactivated enzyme is essentially in the Ni-B state (Fig 5). In recent studies of *Re* MBH[58,61], it has been proposed that two cysteines near the proximal 4Fe-4S cluster contribute to its high redox potential, somehow preventing the formation of the Ni-A state.

The fact that the EPR signal of the reduced 4Fe-4S cluster developed in the case of *Df* V74C in the same potential range as for WT suggests that its potential is not drastically modified, which is not surprising considering the distance to C74. Armstrong and co-workers have proposed on the basis of PFV experiments with the *Av* enzyme that the differential formation of Ni-A/Ni-B depends on electron availability at the active site[8,20]. Under reducing conditions, the Ni-B form would be favoured because oxygen is completely reduced to H_2O and OH^-. Increasing the electrode potential may prevent the complete reduction of O_2, generating reactive oxygen species that would react with the active site to yield the peroxo Ni-A species[13]. In the resistant *Ec*, *Re* and *Aa* enzymes, an additional source of electrons would supply the active site to allow the conversion into the Ni-B species only. Cysteine 74 cannot supply electrons, but we suggest that in the presence of H_2 it accelerates electron transfer from the proximal 4Fe-4S center to the active site so that complete reduction of O_2 can occur. In contrast, in the WT, the formation of Ni-A upon partial reduction of dioxygen is faster than the complete reduction of O_2. This is consistent with the fact that the reduction of Ni-B is much faster in the mutant than in the WT enzyme.

FTIR and PFV experiments show that at a given potential and pH, the Ni-B form of V74C reactivates 17 to 25 times faster than the same species in the WT (Fig 5). The reactivation of Ni-B into Ni-SI, assuming a hydroxyl is bridging Ni and Fe, requires the protonation of this ligand, the one-electron reduction of Ni^{3+} to Ni^{2+} and the departure of the water molecule. A facilitated departure of the produced water molecule seems unlikely since both cysteine, serine and asparagine should induce a more hydrophilic environment. The light-sensitivity process of V74C, which is probably intimately linked to the ability of the active site to exchange protons with its close environment[43], is nearly unaffected, suggesting that the mutation has little effect on proton transfer near the active site. Moreover, the reactivation rates of Ni-B in V74S and V74N are intermediate between WT and V74C (0.11, 0.3, 0.028 and 0.5 s^{-1}, respectively). The pKa of an alcohol and a amide functions being several pH units higher and lower, respectively, than that of the corresponding thiol function, we would not expect such a beneficial effect of the V74S/N mutations if C74 was directly involved in mediating proton transfer. However it is possible that the C74, S74 and N74 mutations ~~facilitates~~ accelerate the protonation of the bridging OH^- ligand through the usual proton pathway but the mechanism remains to be determined. In a previous study, the exponential dependence on electrode potential of the rate of reactivation of Ni-B in *Aa* and *Av* NiFe hydrogenases, showed that an electron transfer step limits the activation of this inactive state[48]. Assuming that an electron transfer step is also rate-determining in the case of the *Df*

enzyme, it is reasonable to assume that this step is faster in V74C (and also in V74S and V74N). Thus the unique conversion into the Ni-B state and the fast reactivation of this state may result from faster electron transfer to the active site.

The mechanism by which the thiol, alcohol and amide functions of V74C, V74S and V74N would accelerate the electron transfer remains to be clarified. Recent studies on synthetic peptides showed that a cysteine can function as a relay which accelerates electron transfer between two redox centers[62,63], but the effect of serine and asparagine has not been reported. The increased in redox potential of the Ni-SI/Ni-B couple, determined by EPR and FTIR-electrochemistry for V74C is small (+15-20 mV) and does not significantly contribute to accelerating electron transfer. It may be that the mutation decreases the reorganization energy or increases the electronic coupling between the proximal cluster and the Ni, which may also substantially change electron transfer rates. Another possibility would be that, according to a coupled electron/proton transfer mechanism, the faster electron transfer in the mutants is conditioned by the prior protonation of the bridging OH^- ligand that would be facilitated by the C74, S74 and N74 mutations. Further experiments are necessary to address these points.

5. Conclusion

The properties of the *Df* V74C mutant (conversion into a Ni-B form that quickly reactivates after O_2 attack, impaired H_2-production activity and weaker affinity for CO) are typical features of the naturally-occuring oxygen-tolerant MBH. From a combination of biochemical, spectroscopic (EPR, FTIR), X-ray and electrochemical studies, we show that C74 favours the formation and the fast reactivation of the Ni-B state. This may result from a faster electron transfer from the FeS clusters to the active site. A fast electron transfer may also occur in the MBH enzymes, although by another mechanism. The comparative study of the *Df* WT, V74C, V74S and V74N and WT *Aa* MBH shows that fast reactivation of the Ni-B state correlates with resistance to O_2. We assume that this will provide further original insights into the mechanism of aerobic (in)activation of [NiFe] hydrogenases. Along with the V74M and V74M/L122M mutants[26], the V74C mutant provides evidence that it is possible to improve the oxygen tolerance of hydrogenases, which is a prerequisite for their biotechnological use in air. Interestingly, the V74C mutant was not designed to copy the sequence of the oxygen resistant enzymes. These results are therefore totally unexpected and they suggest new strategies for conceiving oxygen-tolerant enzymes.

From a practical standpoint, if the aim is to use genetically engineered hydrogenases in biotechnological devices, it is desirable that the mutation that increases oxygen tolerance has no adverse effect on activity. We noted that the V74C mutation does not change the maximal rate of H_2 oxidation, but it increases 60-fold the Michaelis constant for H_2; this is not too problematic because the K_m of the WT being very small (about 10 matm H_2), the turnover rate of V74C under 1 bar H_2 remains close to maximal rate (about 60% of the maximal rate).
The fact that the V74C mutation decreases the hydrogen production rate will limit the use of such variant to H_2 oxidation devices. We note that the oxygen tolerant hydrogenases from *Ralstonia metallidurans* and *R. eutropha* have no H_2 production activity and yet they were successfully used in biofuel cells for generating electricity from H_2 in the presence of O_2 [23,52].

Acknowledgments.

We thank Pr Patrick Bertrand, ~~and~~ Dr Vincent Fourmond, Dr Anne Vobeda and Dr Juan-Carlos Fontecilla-Camps for fruitful discussions. We are grateful to Dr Marie-Thérèse Giudici-Orticoni for providing us the *Aquifex aeolicus* MBH and for helpful discussions. This work was funded by the Centre National de la Recherche Scientifique, Commissariat à l'Energie Atomique, Agence Nationale de la Recherche (Hyliox project), the University of Provence, the City of Marseilles, and the Spanish Ministerio de Ciencia e Innovación (project CTQ2009-12649). This work was supported by the Pôle de Competitivité Capénergies.

Supporting information available:
Activity of *Df* WT and V74C in function of $[O_2]$ determined by HDE experiments in supplementary Figure 1; Potentiometric titrations of the Ni-A/Ni-SU, Ni-B/Ni-SI and $[3Fe\text{-}4S]^+/[3Fe\text{-}4S]^0$ transitions by EPR in supplementary Figure 2; potentiometric titration of the redox states of V74C by FTIR-electrochemistry in supplementary Figure 3; inactivation and reactivation of the WT and V74C enzymes, according to procedures A, B and C described in Materials and Methods in supplementary Figure 4.

References

(1) Tye, J. W.; Hall, M. B.; Darensbourg, M. Y. *Proc Natl Acad Sci U S A* **2005**, *102*, 16911-16912.
(2) Mertens, R.; Liese, A. *Curr Opin Biotechnol* **2004**, *15*, 343-348.
(3) Ghirardi, M. L.; Dubini, A.; Yu, J.; Maness, P. C. *Chem Soc Rev* **2009**, *38*, 52-61.

(4) Magnuson, A.; Anderlund, M.; Johansson, O.; Lindblad, P.; Lomoth, R.; Polivka, T.; Ott, S.; Stensjo, K.; Styring, S.; Sundstrom, V.; Hammarstrom, L. *Acc Chem Res* **2009**, *42*, 1899-1909.

(5) Vignais, P. M.; Billoud, B. *Chem Rev* **2007**, *107*, 4206-4272.

(6) De Lacey, A. L.; Fernandez, V. M.; Rousset, M.; Cammack, R. *Chem Rev* **2007**, *107*, 4304-4330.

(7) Pandelia, M. E.; Fourmond, V.; Tron-Infossi, P.; Lojou, E.; Bertrand, P.; Leger, C.; Giudici-Orticoni, M. T.; Lubitz, W. *J Am Chem Soc* **2010**, *132*, 6991-7004.

(8) Armstrong, F. A.; Belsey, N. A.; Cracknell, J. A.; Goldet, G.; Parkin, A.; Reisner, E.; Vincent, K. A.; Wait, A. F. *Chem Soc Rev* **2009**, *38*, 36-51.

(9) Lukey, M. J.; Parkin, A.; Roessler, M. M.; Murphy, B. J.; Harmer, J.; Palmer, T.; Sargent, F.; Armstrong, F. A. *J Biol Chem* **2010**, *285*, 3928-3938.

(10) Parkin, A.; Goldet, G.; Cavazza, C.; Fontecilla-Camps, J. C.; Armstrong, F. A. *J Am Chem Soc* **2008**, *130*, 13410-13416.

(11) Fernandez, V. M.; Hatchikian, E. C.; Patil, D. S.; Cammack, R. *Biochimica et Biophysica Acta* **1986**, *883*, 145-154.

(12) Pandelia, M. E.; Ogata, H.; Lubitz, W. *Chemphyschem* **2010**, *11*, 1127-1140.

(13) Volbeda, A.; Martin, L.; Cavazza, C.; Matho, M.; Faber, B. W.; Roseboom, W.; Albracht, S. P.; Garcin, E.; Rousset, M.; Fontecilla-Camps, J. C. *J Biol Inorg Chem* **2005**, *10*, 239-249.

(14) Fontecilla-Camps, J. C.; Volbeda, A.; Cavazza, C.; Nicolet, Y. *Chem Rev* **2007**, *107*, 4273-4303.

(15) Ogata, H.; Hirota, S.; Nakahara, A.; Komori, H.; Shibata, N.; Kato, T.; Kano, K.; Higuchi, Y. *Structure* **2005**, *13*, 1635-1642.

(16) Carepo, M.; Tierney, D. L.; Brondino, C. D.; Yang, T. C.; Pamplona, A.; Telser, J.; Moura, I.; Moura, J. J.; Hoffman, B. M. *J Am Chem Soc* **2002**, *124*, 281-286.

(17) Buhrke, T.; Lenz, O.; Krauss, N.; Friedrich, B. *J Biol Chem* **2005**, *280*, 23791-23796.

(18) Duche, O.; Elsen, S.; Cournac, L.; Colbeau, A. *FEBS J* **2005**, *272*, 3899-3908.

(19) Liebgott, P. P.; Leroux, F.; Burlat, B.; Dementin, S.; Baffert, C.; Lautier, T.; Fourmond, V.; Ceccaldi, P.; Cavazza, C.; Meynial-Salles, I.; Soucaille, P.; Fontecilla-Camps, J.; Guigliarelli, B.; Bertrand, P.; Rousset, M.; Léger, C. *Nat Chem Biol* **2010**, *6*, 63-70.

(20) Lamle, S. E.; Albracht, S. P.; Armstrong, F. A. *J Am Chem Soc* **2004**, *126*, 14899-14909.

(21) Cracknell, J. A.; Wait, A. F.; Lenz, O.; Friedrich, B.; Armstrong, F. A. *Proc Natl Acad Sci U S A* **2009**, *106*, 20681-20686.

(22) Leger, C.; Dementin, S.; Bertrand, P.; Rousset, M.; Guigliarelli, B. *J Am Chem Soc* **2004**, *126*, 12162-12172.

(23) Vincent, K. A.; Cracknell, J. A.; Lenz, O.; Zebger, I.; Friedrich, B.; Armstrong, F. A. *Proc Natl Acad Sci U S A* **2005**, *102*, 16951-16954.

(24) Pandelia, M. E.; Infossi, P.; Giudici-Orticoni, M. T.; Lubitz, W. *Biochemistry* **2010**, *49*, 8873-8881.

(25) Lazarus, O.; Woolerton, T. W.; Parkin, A.; Lukey, M. J.; Reisner, E.; Seravalli, J.; Pierce, E.; Ragsdale, S. W.; Sargent, F.; Armstrong, F. A. *J Am Chem Soc* **2009**, *131*, 14154-14155.

(26) Dementin, S.; Leroux, F.; Cournac, L.; De Lacey, A. L.; Volbeda, A.; Léger, C.; Burlat, B.; Martinez, N.; Champ, S.; Martin, L.; Sanganas, O.; Haumann, M.; Fernandez, V. M.; Guigliarelli, B.; Fontecilla-Camps, J.; Rousset, M. *J Am Chem Soc* **2009**, *131*, 10156-10164.

(27) Leroux, F.; Dementin, S.; Burlat, B.; Cournac, L.; Volbeda, A.; Champ, S.; Martin, L.; Guigliarelli, B.; Bertrand, P.; Fontecilla-Camps, J.; Rousset, M.; Léger, C. *Proc Natl Acad Sci U S A* **2008**, *105*, 11188-11193.

(28) Cournac, L.; Guedeney, G.; Peltier, G.; Vignais, P. M. *J Bacteriol* **2004**, *186*, 1737-1746.

(29) Jones, A. K.; Lamle, S. E.; Pershad, H. R.; Vincent, K. A.; Albracht, S. P.; Armstrong, F. A. *J Am Chem Soc* **2003**, *125*, 8505-8514.

(30) Fourmond, V.; Lautier, T.; Baffert, C.; Leroux, F.; Liebgott, P. P.; Dementin, S.; Rousset, M.; Arnoux, P.; Pignol, D.; Meynial-Salles, I.; Soucaille, P.; Bertrand, P.; Léger, C. *Anal Chem* **2009**, *81*, 2962-2968.

(31) Fourmond, V.; Hoke, K.; Heering, H. A.; Baffert, C.; Leroux, F.; Bertrand, P.; Leger, C. *Bioelectrochemistry* **2009**.

(32) Dementin, S.; Burlat, B.; De Lacey, A. L.; Pardo, A.; Adryanczyk-Perrier, G.; Guigliarelli, B.; Fernandez, V. M.; Rousset, M. *J Biol Chem* **2004**, *279*, 10508-10513.

(33) De Lacey, A. L.; Stadler, C.; Fernandez, V. M.; Hatchikian, E. C.; Fan, H. J.; Li, S.; Hall, M. B. *J Biol Inorg Chem* **2002**, *7*, 318-326.

(34) Volbeda, A.; Garcin, E.; Piras, C.; De Lacey, A. L.; Fernandez, V. M.; Hatchikian, C. E.; Frey, M.; Fontecilla-Camps, J. C. *J Am Chem Soc* **1996**, *118*, 12989-12996.

(35) Volbeda, A.; Montet, Y.; Vernede, X.; Hatchikian, E. C.; Fontecilla-Camps, J. C. *Int J Hydrogen Energ* **2002**, *27*, 1449-1461.

(36) Kabsch, W. *Acta Crystallogr D Biol Crystallogr* **2010**, *66*, 125-132.

(37) McCoy, A. J.; Grosse-Kunstleve, R. W.; Adams, P. D.; Winn, M. D.; Storoni, L. C.; Read, R. J. *J Appl Crystallogr* **2007**, *40*, 658-674.

(38) Murshudov, G. N.; Vagin, A. A.; Dodson, E. J. *Acta Crystallogr D Biol Crystallogr* **1997**, *53*, 240-255.

(39) Winn, M. D.; Isupov, M. N.; Murshudov, G. N. *Acta Crystallogr D Biol Crystallogr* **2001**, *57*, 122-133.

(40) Emsley, P.; Lohkamp, B.; Scott, W. G.; Cowtan, K. *Acta Crystallogr D Biol Crystallogr*, *66*, 486-501.

(41) Guigliarelli, B.; More, C.; Fournel, A.; Asso, M.; Hatchikian, E. C.; Williams, R.; Cammack, R.; Bertrand, P. *Biochemistry* **1995**, *34*, 4781-4790.

(42) Medina, M.; Hatchikian, E. C.; Cammack, R. *Biochim Biophys Acta* **1996**, *1275*, 227-236.

(43) Dole, F.; Medina, M.; More, C.; Cammack, R.; Bertrand, P.; Guigliarelli, B. *Biochemistry* **1996**, *35*, 16399-16406.

(44) Rousset, M.; Montet, Y.; Guigliarelli, B.; Forget, N.; Asso, M.; Bertrand, P.; Fontecilla-Camps, J. C.; Hatchikian, E. C. *Proc Natl Acad Sci U S A* **1998**, *95*, 11625-11630.

(45) Asso, M.; Guigliarelli, B.; Yagi, T.; Bertrand, P. *Biochim Biophys Acta* **1992**, *1122*, 50-56.

(46) De Lacey, A. L.; Fernandez, V. M.; Rousset, M.; Cavazza, C.; Hatchikian, E. C. *J Biol Inorg Chem* **2003**, *8*, 129-134.

(47) Fernandez, V. M.; Hatchikian, E. C.; Cammack, R. *Biochim Biophys Acta* **1985**, *832*, 69-79.

(48) Fourmond, V.; Infossi, P.; Giudici-Orticoni, M. T.; Bertrand, P.; Leger, C. *J Am Chem Soc* **2010**, *132*, 4848-4857.

(49) Bleijlevens, B.; van Broekhuizen, F. A.; De Lacey, A. L.; Roseboom, W.; Fernandez, V. M.; Albracht, S. P. *J Biol Inorg Chem* **2004**, *9*, 743-752.

(50) Leger, C.; Jones, A. K.; Roseboom, W.; Albracht, S. P.; Armstrong, F. A. *Biochemistry* **2002**, *41*, 15736-15746.

(51) Guiral, M.; Tron, P.; Belle, V.; Aubert, C.; Leger, C.; Guigliarelli, B.; Giudici-Orticoni, M. T. *Int J Hydrogen Energ* **2006**, *31*, 1424-1431.

(52) Vincent, K. A.; Cracknell, J. A.; Clark, J. R.; Ludwig, M.; Lenz, O.; Friedrich, B.; Armstrong, F. A. *Chem Commun (Camb)* **2006**, 5033-5035.

(53) Krassen, H.; Schwarze, A.; Friedrich, B.; Ataka, K.; Lenz, O.; Heberle, J. *ACS Nano* **2009**, *3*, 4055-4061.

(54) Reisner, E.; Powell, D. J.; Cavazza, C.; Fontecilla-Camps, J. C.; Armstrong, F. A. *J Am Chem Soc* **2009**, *131*, 18457-18466.

(55) Ihara, M.; Nishihara, H.; Yoon, K. S.; Lenz, O.; Friedrich, B.; Nakamoto, H.; Kojima, K.; Honma, D.; Kamachi, T.; Okura, I. *Photochem Photobiol* **2006**, *82*, 676-682.

(56) Ludwig, M.; Cracknell, J. A.; Vincent, K. A.; Armstrong, F. A.; Lenz, O. *J Biol Chem* **2009**, *284*, 465-477.

(57) Leroux, F.; Liebgott, P. P.; Cournac, L.; Richaud, P.; Kpebe, A.; Burlat, B.; Guigliarelli, B.; P., B.; Leger, C.; Rousset, M.; Dementin, S. *Int J Hydrogen Energ* **2010**, *35*, 10770-10777.

(58) Lenz, O.; Ludwig, M.; Schubert, T.; Burstel, I.; Ganskow, S.; Goris, T.; Schwarze, A.; Friedrich, B. *Chemphyschem* **2010**, *11*, 1107-1119.

(59) Leger, C.; Bertrand, P. *Chem Rev* **2008**, *108*, 2379-2438.

(60) Pandelia, M. E.; Infossi, P.; Giudici-Orticoni, M. T.; Lubitz, W. *Biochemistry* **2010**, *in press*.

(61) Saggu, M.; Zebger, I.; Ludwig, M.; Lenz, O.; Friedrich, B.; Hildebrandt, P.; Lendzian, F. *J Biol Chem* **2009**, *284*, 16264-16276.

(62) Wang, M.; Gao, J.; Muller, P.; Giese, B. *Angew Chem Int Ed Engl* **2009**, *48*, 4232-4234.

(63) Giese, B.; Wang, M.; Gao, J.; Stoltz, M.; Muller, P.; Graber, M. *J Org Chem* **2009**, *74*, 3621-3625.

Figure captions

Figure 1
Structure of the [NiFe] hydrogenase from *D. fructosovorans* at 1.8Å resolution (pdb 1YQW). The gas channel is depicted in grey. The position of V74 is indicated in the inset.

Figure 2

Effect of O_2 addition on the H/D exchange reaction catalyzed by WT and V74C hydrogenases. In the presence of D-labelled hydrogen (99% D_2), following anoxia establishment and enzyme activation by reduced methyl viologen (MV_{red}), unlabelling occurs resulting in an increase of H_2 and HD proportions. Injection of air-saturated water up to reaching *ca* 8 µM O_2 completely stops enzyme activity in WT, whereas in V74C an O_2 consumption followed by a restoration of HDE are observed.

Figure 3

EPR signatures of the NiFe center in V74C and WT hydrogenases. EPR spectra of the oxidized (a, b and e traces) and reduced (c and d) enzymes were recorded at the temperature of 100K, microwave power 10mW, modulation amplitude 1mT (a,b) 100K, 10mW, 0,2mT (e) 70K, 10mW, 1mT (c, d). Microwave frequency: ν = 9.4059 GHz. Protein concentrations were about 30-50 µM, depending on the sample. The usual Ni signatures include the Ni-A species at g = 2.31, 2.23, 2.01 and the Ni-B species at g = 2.33, 2.16, 2.01. An additional signal at 2.11, 2.10, 2.01 (traces b and e) that accounts for about 0.03 spin/enzyme in the spectrum displayed in trace b and which proportion varies between 0.01 to 0.07 spin/enzyme depending on preparation. The reduced Ni-C states (traces c and d) were obtained i) by adding a small aliquot of a concentrated sodium dithionite solution (100mM in 50mM Hepes buffer at pH 8.0) to the oxidised WT sample, ii) by keeping overnight the oxidised V74C sample in a glovebox filled with N_2 and traces of H_2.

Figure 4

FTIR spectra of [NiFe] hydrogenases from *D. fructosovorans* poised in a spectroelectrochemical cell at different redox potentials. **A.** 0.7 mM wild type enzyme: a) as-prepared, open circuit potential was +230 mV, 25ºC; b) -280 mV, 5ºC; c) at -495 mV, 25ºC, after activation (activation was achieved at -295 mV, 25ºC, during 210 min; d) -395 mV, 25ºC, after activation; e) -245 mV, 25ºC; f) -5 mV, 40ºC, 30 min. **B.** 1.1 mM V74C mutant:

g) as-prepared, open circuit potential was +275 mV, 25ºC; h) -305 mV, 5ºC; i) at -555 mV, 25ºC, after activation (activation was achieved at -555 mV, 25ºC, during 180 min; j) -425 mV, 25ºC, after activation; k) -325 mV, 25ºC; l) -5 mV, 25ºC, 8 min.

Figure 5

Reactivation of the WT (red), V74C (purple), V74S (cyan, panel A only) and V74N (green, panel A only) enzymes, at -90mV, pH 5.5, 1 atm of H_2, after the enzymes have been inactivated according to either of the three procedures described in the Material and Methods and supplementary fig S4.

A: reactivation after anaerobic inactivation at +90mV under 1 bar H_2, according to procedure A.

B: reactivation after aerobic inactivation at -90mV, under 1 atm of H_2, according to procedure B.

C: reactivation after aerobic inactivation at +215mV, under 1 atm of Ar, according to procedure C.

The dashed lines show the best fit to eq (1) and (3) for the V74C and WT enzymes, respectively, from which the values of τ fast could be determined.

Figure 6

Cyclic voltammograms recorded with WT (red), V74C (purple), V74S (cyan) and V74N (green) [NiFe] hydrogenases adsorbed at a rotating pyrolytic graphite edge electrode. Scan rate 0.3mV/s, pH 5.5, 40°C, 1atm of H_2, electrode rotation rate 2 krpm. Arrows indicate the directions of the sweeps; vertical arrows mark the values of Esw.

Figure 7

FTIR spectra of [NiFe] hydrogenases from *D. fructosovorans* under different conditions.

A. 0.10 mM wild type enzyme: a) as isolated aerobically; b) after 4 hours under 1 atm H_2, 25ºC; c) after reoxidation with air. B. 0.06 mM V74C mutant: d) as isolated aerobically; e) after 4 hours under 1 atm H_2 , 25ºC; f) after reoxidation with air.

Figure 8

Anaerobic and aerobic inhibition of WT (red), V74C, (purple), V74S (cyan) and V74N (green) hydrogenases adsorbed at a rotating electrode poised at +140mV, 40°C, pH5.5, 1 atm H_2. (A) Oxygen concentration in the cell during experiment. The three peaks correspond to

injections of 100, 200 and 500 µl of an air-saturated solution (B) Effect of O_2 on enzyme's activity. The traces were recorded after a 200s (WT) or 500s (V74C) poise at +140 mV. (C) Anaerobic inactivation of V74C adsorbed at a rotating electrode poised at +140mV, 40°C, pH5.5, 1 atm H_2 from an independent experiment. The dashed black line is a fit to eq 4, from which the value of τ fast could be measured. (D) Zoom on the inactivation/reactivation of V74C during exposure to 20 µM O_2. The black line is a fit to a simple exponential function.

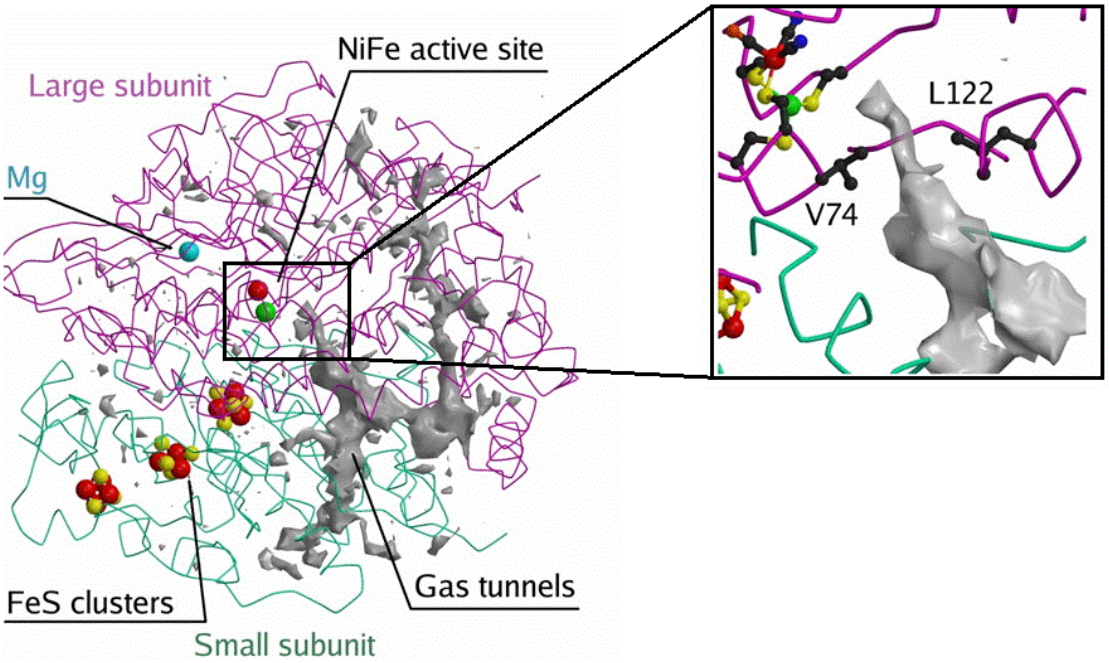
NiFe active site
Large subunit
Mg
L122
V74
FeS clusters
Gas tunnels
Small subunit

Figure 1

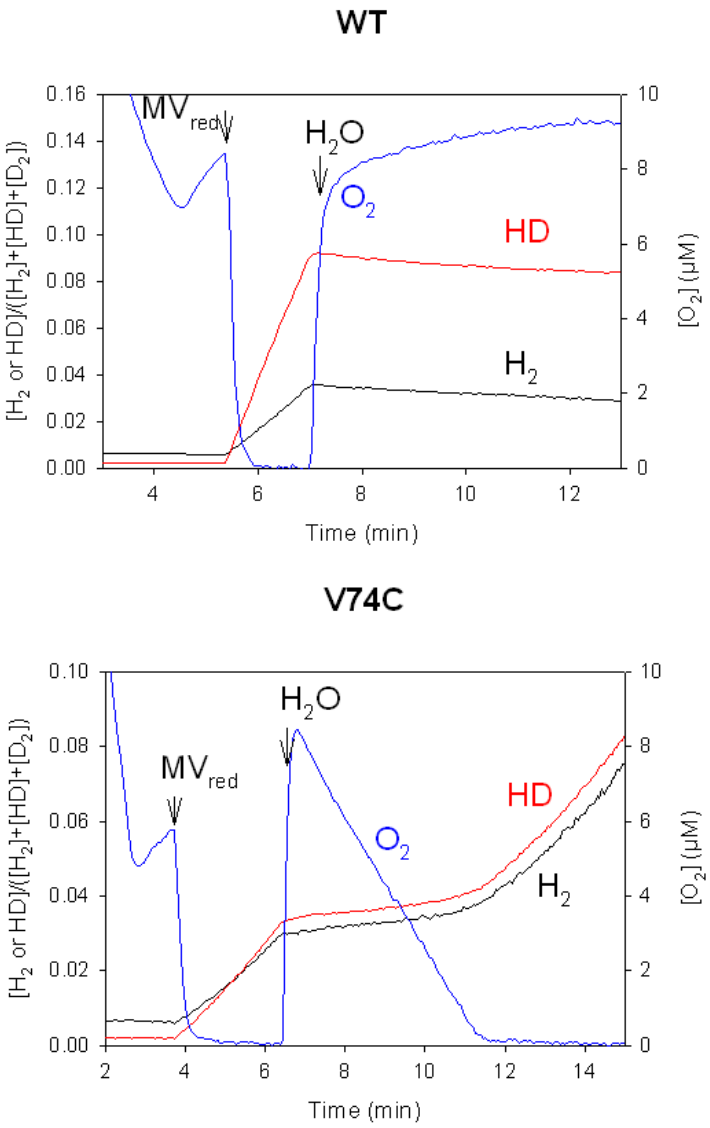
WT
MV red
H2O
O2
HD
H2
[H2 or HD]/([H2]+[HD]+[D2])
[O2] (μM)
Time (min)
V74C
MV red
H2O
O2
HD
H2
[H2 or HD]/([H2]+[HD]+[D2])
[O2] (μM)
Time (min)

Figure 2

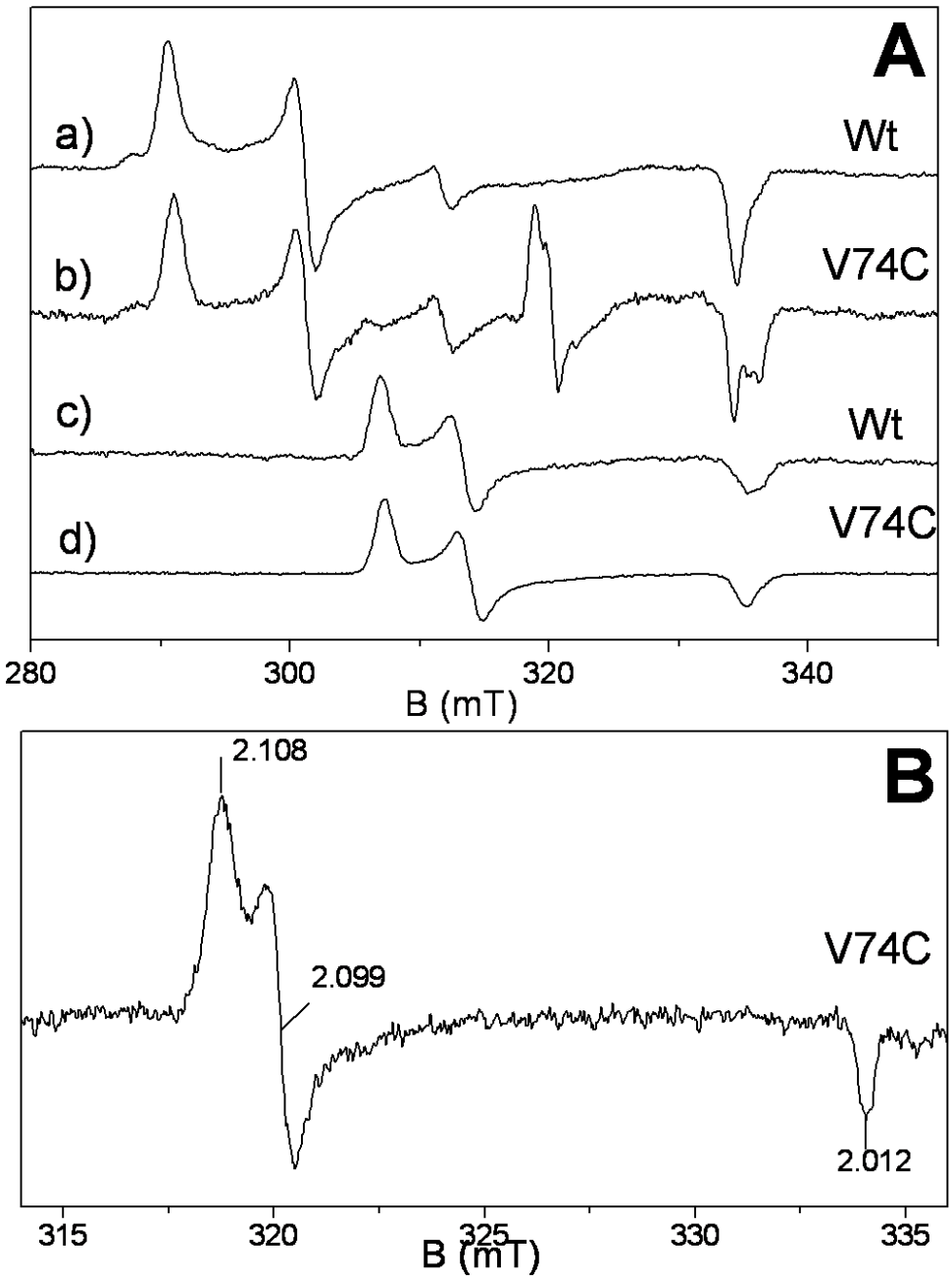
A
a)
Wt
b)
V74C
c)
Wt
d)
V74C
280
300
320
340
B (mT)
B
2.108
V74C
2.099
2.012
315
320
325
330
335
B (mT)

Figure 3

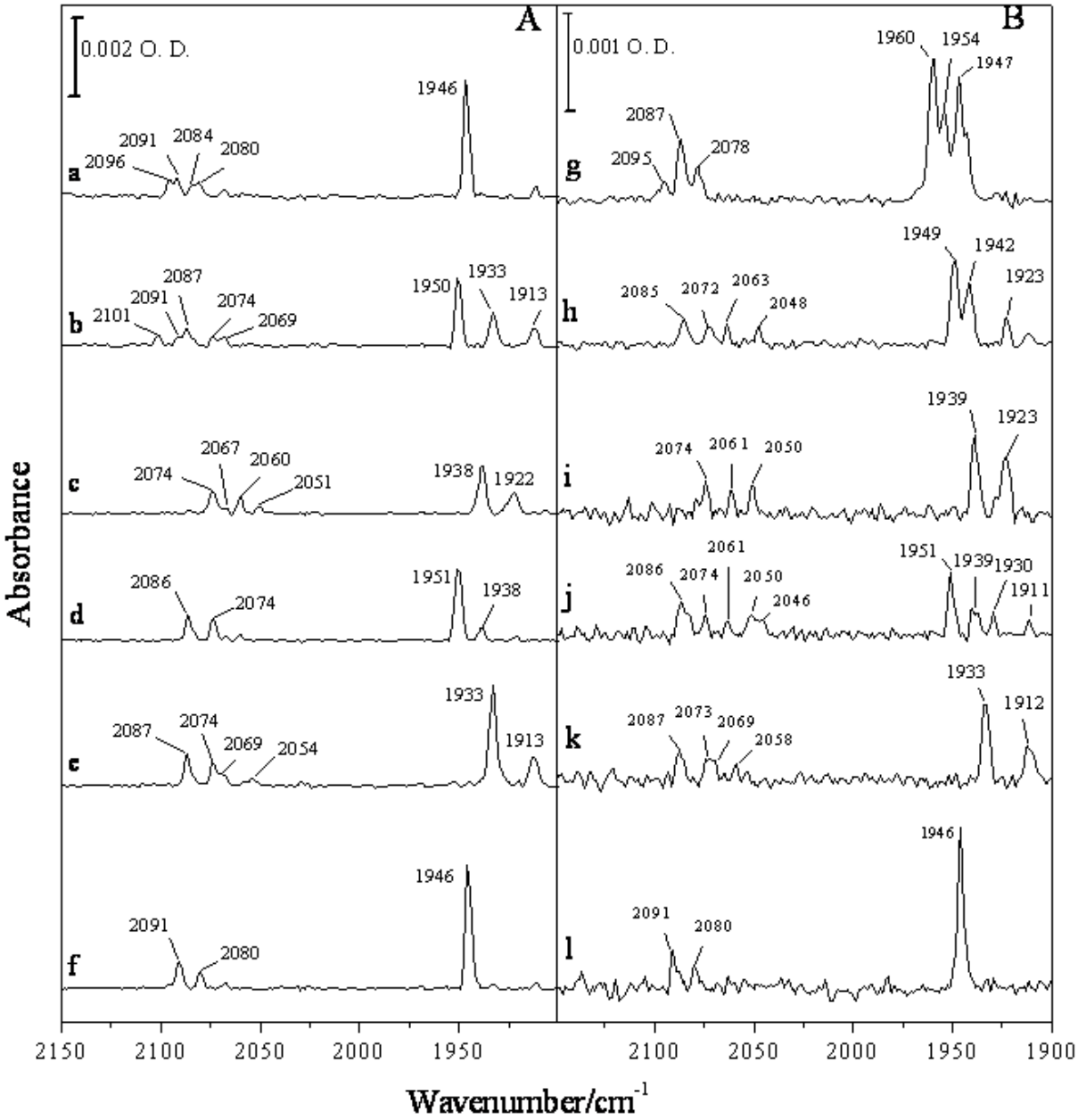
A
B
0.002 O. D.
0.001 O. D.
a
b
c
d
e
f
g
h
i
j
k
l
2096
2091
2084
2080
1946
2101
2091
2087
2074
2069
1950
1933
1913
2074
2067
2060
2051
1938
1922
2086
2074
1951
1938
2087
2074
2069
2054
1933
1913
2091
2080
1946
2095
2087
2078
1960
1954
1947
2085
2072
2063
2048
1949
1942
1923
2074
2061
2050
1939
1923
2086
2074
2061
2050
2046
1951
1939
1930
1911
2087
2073
2069
2058
1933
1912
2091
2080
1946
Absorbance
2150
2100
2050
2000
1950
2100
2050
2000
1950
1900
Wavenumber/cm-1

Figure 4

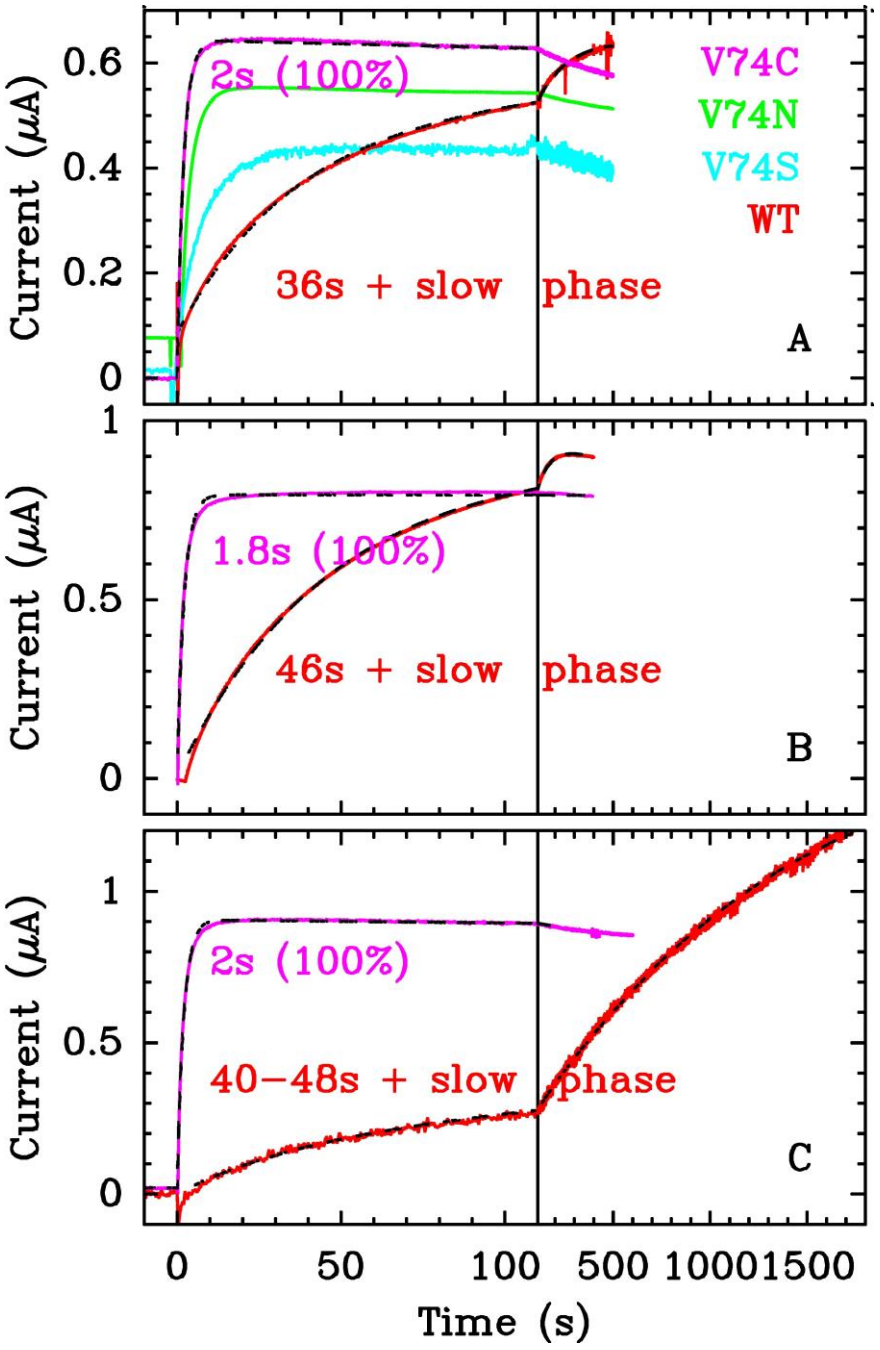
Current (μA)
0.6
0.4
0.2
0
2s (100%)
V74C
V74N
V74S
WT
36s + slow phase
A
1
0.5
0
1.8s (100%)
46s + slow phase
B
1
0.5
0
2s (100%)
40−48s + slow phase
C
0
50
100
500
1000
1500
Time (s)

Figure 5

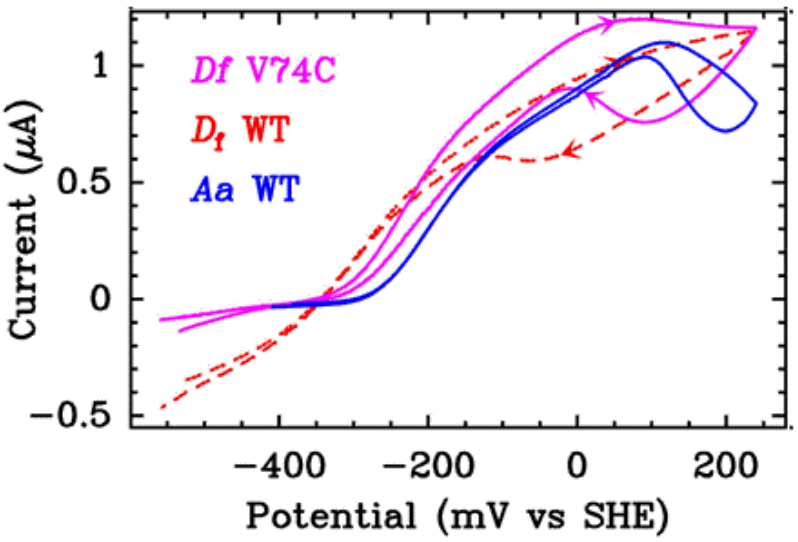
Df V74C
Df WT
Aa WT
Current (μA)
1
0.5
0
−0.5
−400
−200
0
200
Potential (mV vs SHE)

Figure 6

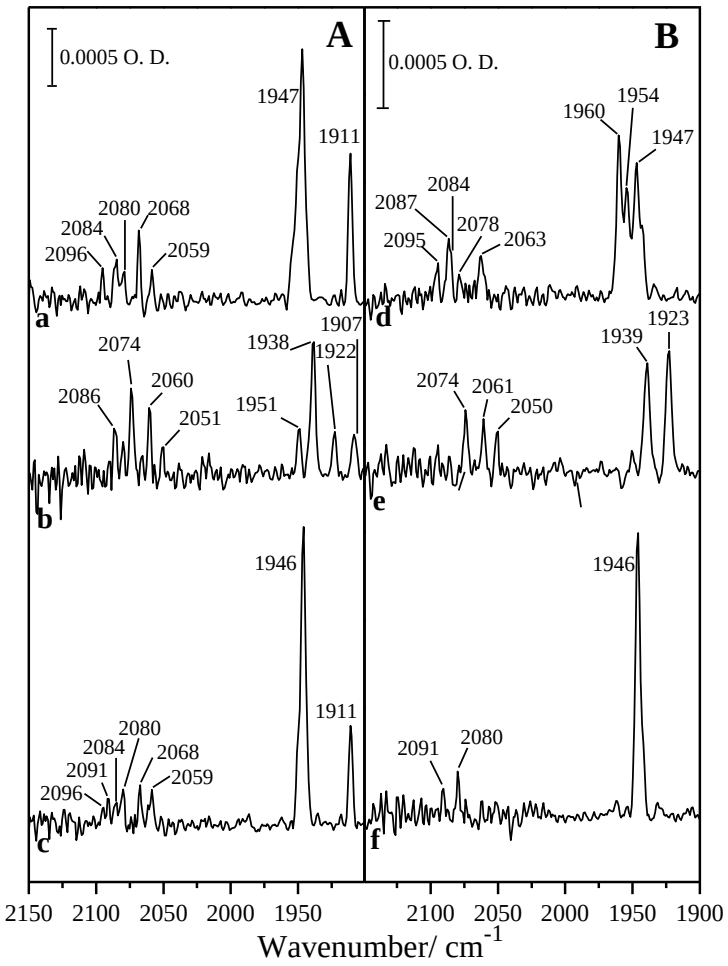
A
B
0.0005 O. D.
0.0005 O. D.
1947
1911
2080
2068
2084
2096
2059
1960
1954
1947
2087
2084
2078
2095
2063
a
d
2074
1938
1907
1922
2086
2060
2051
1951
2074
2061
2050
1939
1923
b
e
1946
1946
1911
2080
2084
2068
2091
2059
2096
2091
2080
c
f
2150 2100 2050 2000 1950
2100 2050 2000 1950 1900
Wavenumber/ cm-1

Figure 7

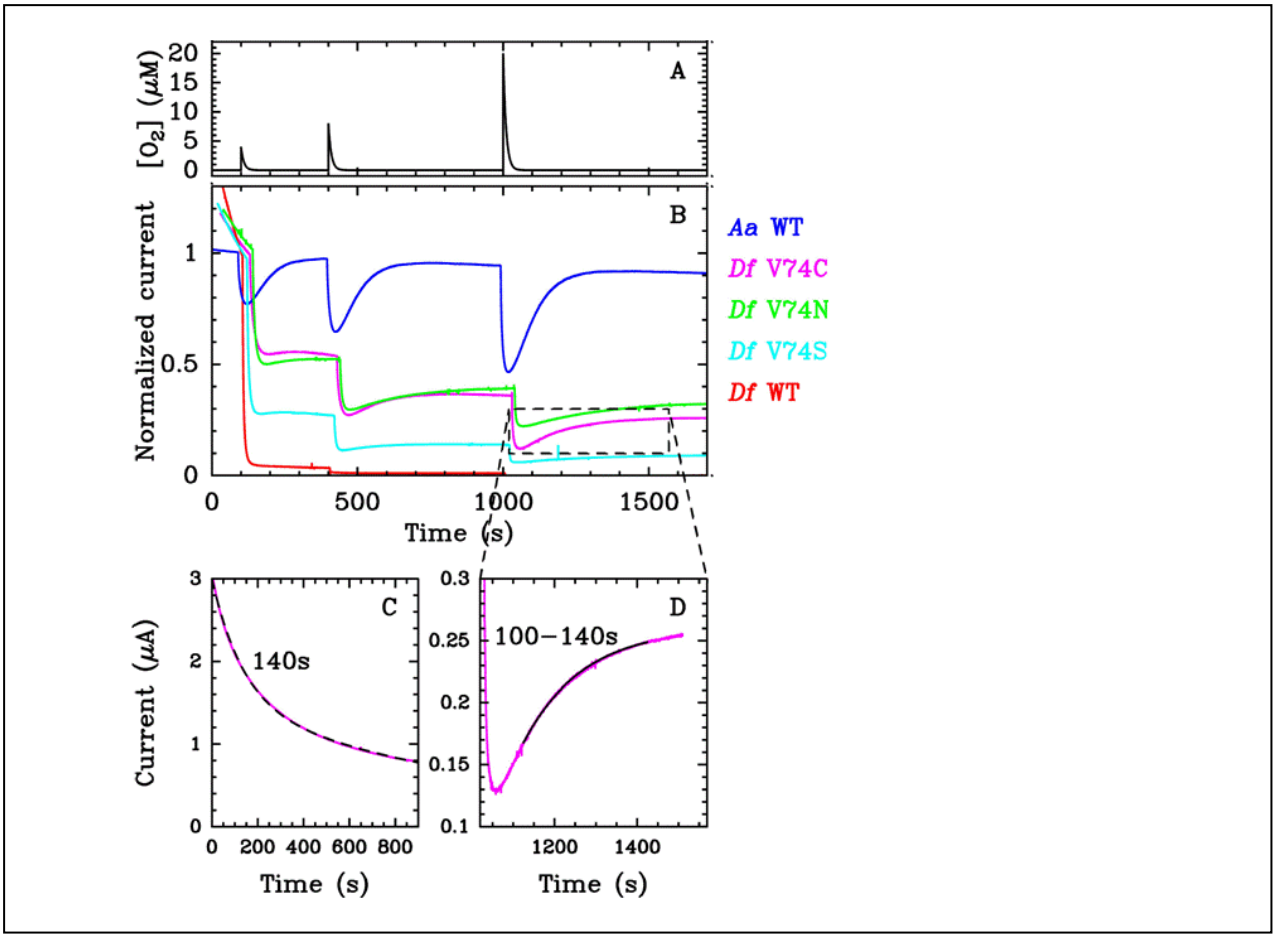
A
B
C
D
[O2] (μM)
Normalized current
Time (s)
Current (μA)
140s
100−140s
Aa WT
Df V74C
Df V74N
Df V74S
Df WT

Figure 8

Supplementary Figure S1 :

Residual activity (rate of O_2 consumption + rate of H/D exchange) determined by the HDE assay in the presence of different [O_2].

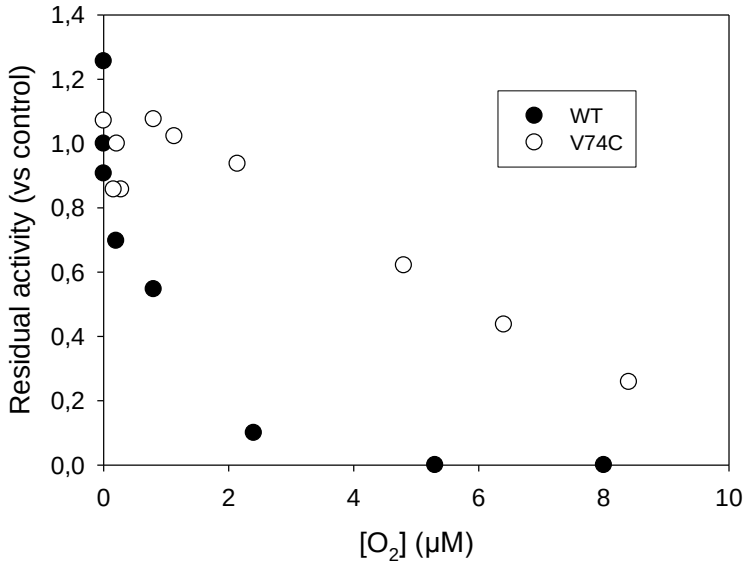

Supplementary Figure S2

Reductive titration of the V74C mutant by EPR at 27°C and pH 8. The normalised peak-to-peak amplitudes (g_{3Fe4S} = 2.02, $g_{y,\ Ni\text{-}A}$ = 2.23, $g_{y,\ Ni\text{-}B}$ = 2.16) are plotted against the redox potential.

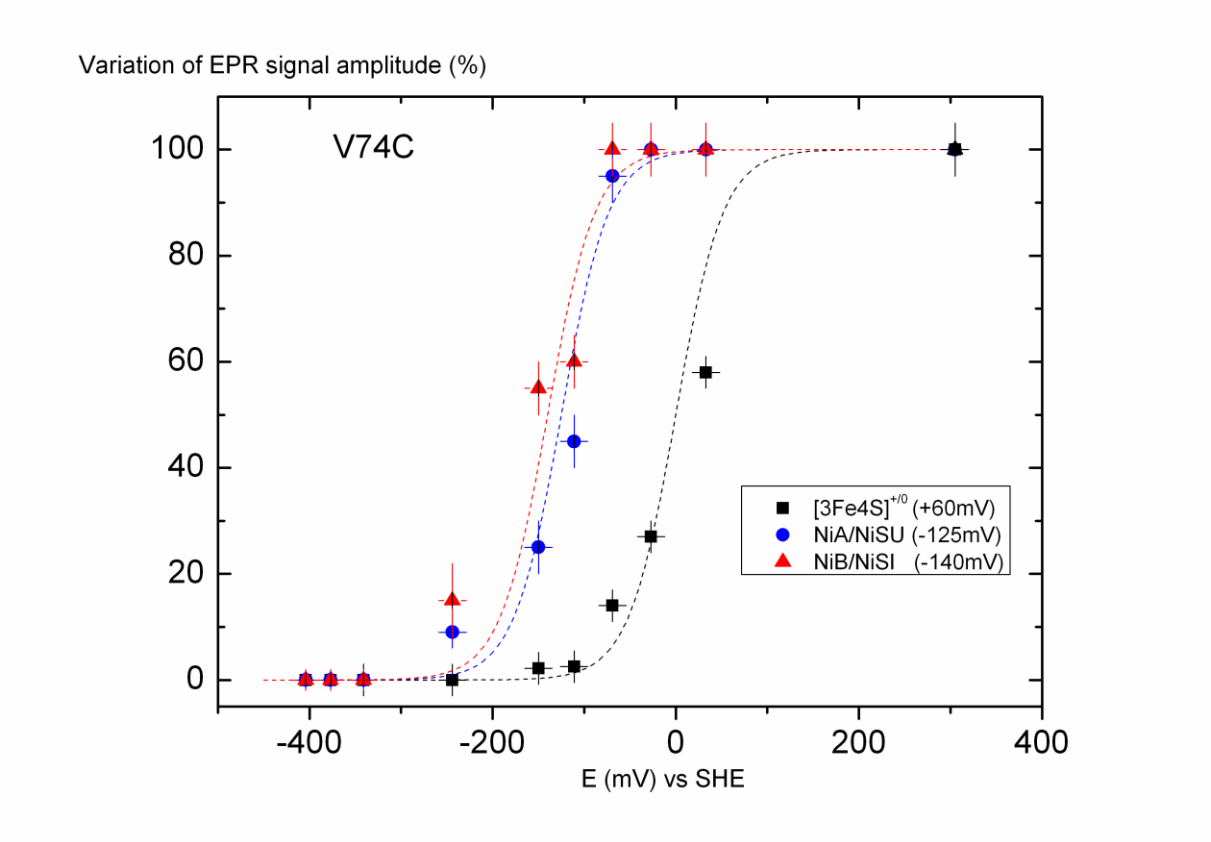

Supplementary Figure S3

Potentiometric titration of the redox states of V74C by FTIR-electrochemistry at 25°C, pH 8. The apparent intensity of the CO bands of the different states is plotted against the redox potential. A. Ni-A (closed circles) and Ni-SU (open circles), B. Ni-B (closed circles) and Ni-SI (open circles), C. New as-prepared 1960 and 1954 cm^{-1} CO bands (closed circles) and Ni-R (open circles), D. Ni-SI (closed circles), Ni-C (open circles) and Ni-R (closed triangles)

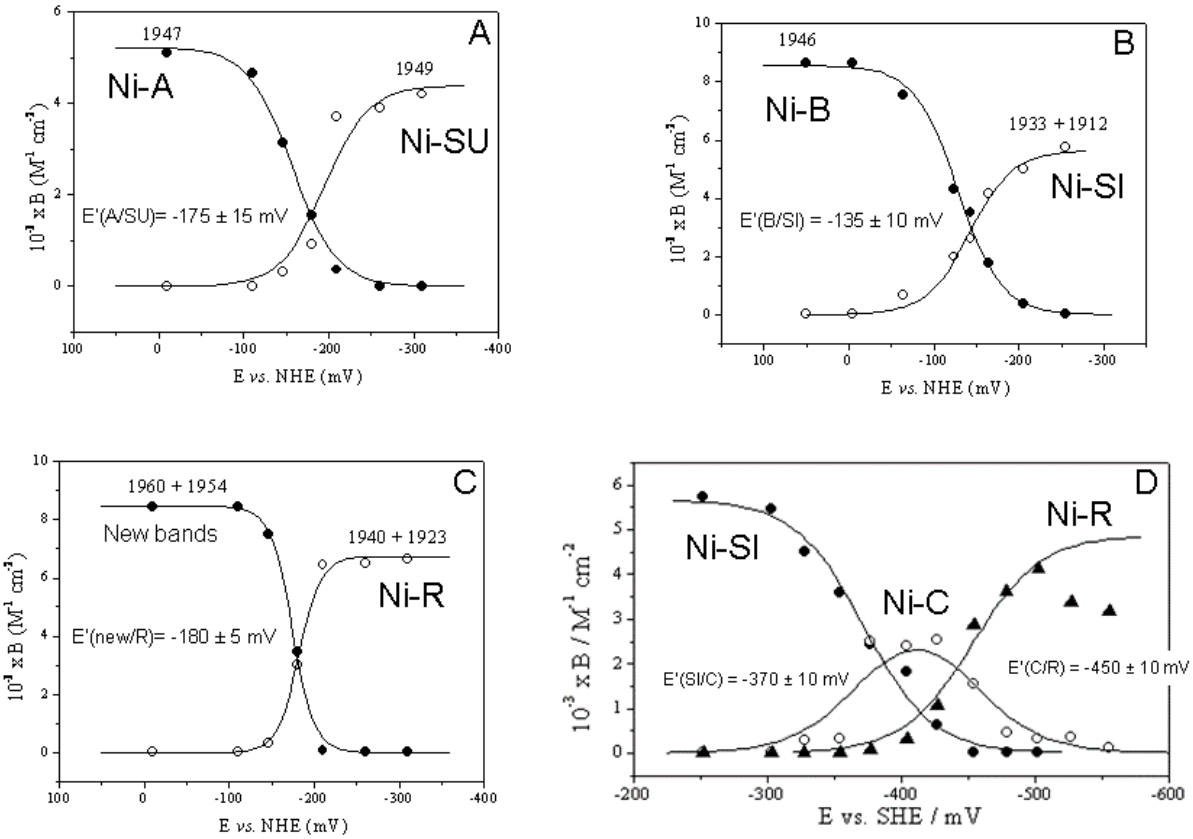

Supplementary Figure S4

Inactivation and reactivation of the WT (red) and V74C (purple) enzymes, according to procedures A, B and C (panels A, B and C, respectively). The reactivations are those shown in Fig 3A-3C. pH 5.5, 40°C. See materials and methods for details.